

## Accepted Manuscript

Multi-criteria optimization of a micro solar-geothermal CCHP system applying water/CuO nanofluid based on exergy, exergoeconomic and exergoenvironmental concepts

Fateme Ahmadi Boyaghchi, Mansoure Chavoshi

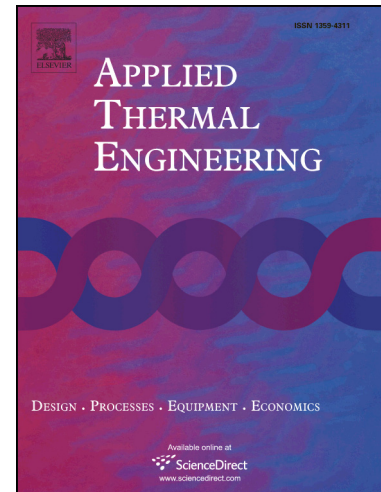
PII: S1359-4311(16)32661-8  
DOI: <http://dx.doi.org/10.1016/j.applthermaleng.2016.10.139>  
Reference: ATE 9341

To appear in: *Applied Thermal Engineering*

Received Date: 22 February 2016  
Revised Date: 26 September 2016  
Accepted Date: 22 October 2016

Please cite this article as: F. Ahmadi Boyaghchi, M. Chavoshi, Multi-criteria optimization of a micro solar-geothermal CCHP system applying water/CuO nanofluid based on exergy, exergoeconomic and exergoenvironmental concepts, *Applied Thermal Engineering* (2016), doi: <http://dx.doi.org/10.1016/j.applthermaleng.2016.10.139>

This is a PDF file of an unedited manuscript that has been accepted for publication. As a service to our customers we are providing this early version of the manuscript. The manuscript will undergo copyediting, typesetting, and review of the resulting proof before it is published in its final form. Please note that during the production process errors may be discovered which could affect the content, and all legal disclaimers that apply to the journal pertain.



**In Multi-criteria optimization of a micro solar-geothermal CCHP system  
applying water/CuO nanofluid based on exergy, exergoeconomic and  
exergoenvironmental concepts**

**Fateme Ahmadi Boyaghchi<sup>\*,1</sup>**

<sup>1</sup> Department of Mechanical Engineering, Faculty of Engineering & Technology, Alzahra University, Deh-Vanak, Tehran, Iran.

**\*Corresponding author:**

**Tel.:** +9821 88044040 2140

**Fax:** +9821 88617537

**E-mail:** [fahmadi@alzahra.ac.ir](mailto:fahmadi@alzahra.ac.ir),

[aboyaghchi@gmail.com](mailto:aboyaghchi@gmail.com)

**Mansoure Chavoshi<sup>1</sup>**

<sup>1</sup> Department of Mechanical Engineering, Faculty of Engineering & Technology, Alzahra University, Deh-Vanak, Tehran, Iran.

**Abstract**

The main objective of the present study is to perform the thermodynamic, economic and environmental analyses of a solar-geothermal driven combined cooling, heating and power (CCHP) cycle integrated with flat plate collectors containing water/copper oxide (CuO) nanofluid as the absorbing medium. Twelve main parameters are selected as the decision variables of the desired system while the daily exergetic efficiency, total product cost rate and total product environmental impact associated with exergy rate are chosen as the three main objective functions. NSGA-II (Non-dominated Sort Genetic Algorithm-II) is individually applied to obtain the final optimal solutions in the multi-objective optimization of the desired system for four working fluids including R134a, R423A, R1234ze and R134yf from the exergy, exergoeconomic and exergoenvironmental points of view. Based on the multi-objective optimization outcomes, R1234ze is the best fluid with 36.82 Pts/h total product environmental impact rate so that the maximum nanoparticles volume fraction and minimum collector tilt angle are required. Moreover, R423A with the minimum total product cost rate of 4496 \$/year is the best fluid at which minimum collector area is needed. Furthermore, R134a is the best fluid with 4.194% daily exergetic efficiency so that the minimum nanoparticle volume fraction is required compared with other studied fluids.

**Keywords:** Flat plate collector, Organic Rankine cycle, Ejector refrigeration, water/CuO nanofluid, Environmental impact, NSGA-II.

## Introduction

One possible developmental path is decentralization of the electricity system. Distributed power generation in small, decentralized units is expected to help in reducing emissions and saving grid capacity, while also providing opportunities for renewable energy [1]. Applying geothermal energy as well as the thermoeconomic method to analyze the energy systems have been considered by several researchers. Performance assessment of a horizontal ground source heat pump with R22 as working fluid for a heating mode and comparison of its cost effectiveness with those of conventional heating methods were carried out by Esen et al. [2]. They compared a ground-coupled heat pump with an air-coupled heat pump system from the thermoeconomical viewpoint. The test results indicated that system parameters can have an important effect on the performance, and that ground-coupled heat pump systems were economically preferable to air-coupled heat pump systems for the purpose of space cooling [3]. Moreover, energetic and exergetic analyses of ground-coupled heat pump system with two different horizontal ground heat pumps were performed and the influences of the buried depth of the earth coupled heat exchanger on the energetic and exergetic efficiencies were conducted [4]. Esen and Yuksel [5] depicted that some renewable energy namely geothermal and solar energies can be effectively employed to heat a greenhouse during the typical winter conditions in eastern Turkey.

Additionally, an increasing issue is paid to CCHP system due to its environment-friendly, operation cost saving and energy saving characteristics [6]. One objective of CCHP systems is the diversification of energy sources, especially use of renewable ones, accordingly to the geographical location and possibilities [7]. This system is widely studied and optimized thermodynamically and thermoeconomically by researchers. Wang et al. [8] proposed a new solar CCHP based on a Rankine cycle and an ejector refrigeration cycle. The effects of hour

angle and the slope angle of the collector aperture on the system performance were examined and genetic algorithm applied to find the maximum exergy efficiency. Zhai et al. [9] proposed and extensively investigated a hybrid solar CCHP system integrated with parabolic trough solar collector. An annual energy and exergy efficiencies of the system were evaluated under the climate of northwestern region of China. Meng et al. [10] presented a new CCHP system driven by solar energy and industrial waste heat. Two pairs of metal hydrides were selected and the working principle of the system was discussed for the proposed system. The multi-element valued method was used to evaluate the performance of the system in a whole sense. Balli et al. [11] provided thermodynamic and thermoeconomic methodologies for a CCHP system with a gas-diesel engine. They apply the developed methodologies to an actual CCHP system with a rated output of 6.5MW gas-diesel engine installed in the Eskisehir Industry Estate Zone, Turkey. Several thermodynamic performance parameters namely energy and exergy efficiencies, equivalent electrical efficiency, the Public Utility Regulatory Policies Act efficiency, fuel energy saving ratio, fuel exergy saving ratio and other were determined for the desired system [12]. A complementary CCHP based on ORC system and its optimal operation strategy were presented in Ref.[13] in order to solve the randomness of load demands. Wang et al. [14] proposed a new solar driven CCHP system combining a Brayton cycle and a transcritical CO<sub>2</sub> refrigeration cycle with ejector-expansion device. Parametric study was carried out to assess the effect of major parameters on the exergy efficiency. Mago et al. [15] conducted an analysis to determine the economic, energetic, and environmental potential benefits that can be obtained from the implementation of a combined micro-turbine ORC versus a simple micro-turbine or a topping-cycle combined heat and power system. Ghaebi et al. [16] considered the cost rate of product of a gas turbine CCHP system as an objective function and applied genetic algorithm technique to

find the optimum operating of system. Al-Sulaiman et al. [17, 18] presented and examined the thermoeconomic optimization formulations of three new ORC-CCHP systems, i.e. SOFC-CCHP, biomass-CCHP, and solar-CCHP systems. Results showed the better performance for SOFC-CCHP from the exergy viewpoint while the cost per exergy unit for solar-CCHP was obtained less than that for other systems. Guo et al. [19] presented a two-stage optimal planning and design method for CCHP microgrid system. NSGA-II method was applied to solve the optimal design problem including the optimization of equipment type and capacity and mixed-integer linear programming algorithm was used to solve the optimal dispatch problem. Sanaye and Hajabdollahi [20] modeled and optimized a solar assisted CCHP plant. Both the genetic algorithm and particle swarm optimization were used to maximize the actual annual benefit. Boyaghchi and Heidarnejad [21, 22] proposed and optimized a new CCHP system integrated with evacuated tube solar collectors based on ORC for two summer and winter. Thermal and exergy efficiencies as well as total product cost rate were selected as the objective functions. Wang et al. [23] thermodynamically performed and optimized a solar driven CCHP system for three modes, i.e. power, cooling and power and heating and power. The average useful output and the total heat transfer area were selected as two objective functions and NSGA-II technique was applied to find the optimal operation of desired system.

Besides the exergy and exergoeconomic methods, exergoenvironmental analysis, a combination of exergy analysis and life cycle assessment (LCA) principles, is a relatively new method to evaluate the environmental impacts of energy conversion systems, such as, the high-temperature solid oxide fuel cell [24], the vapor methane reform process for hydrogen production [25], the oxy-fuel power plant with CO<sub>2</sub> capture and without CO<sub>2</sub> capture [26, 27], the turboprop engine used in district airplanes [28], the traditional coal boiler, condensing natural gas combi

boiler [29], the reverse osmosis sea water purification plant [30], the hybrid electrical vehicle thermal direction system [31], the gas fired steam power plant [32], geothermal district heating system [33], the cogeneration system based on Organic Rankine cycle used in cement industry [34] and an air conditioning system [35].

To the best of our knowledge, there is no study reported in the literature on evaluation and multi objective optimization of CCHP system based on the exergoenvironmental concept. The objective of the current study is to propose and model a new hybrid solar-geothermal driven CCHP system with the ejector refrigeration cycle, integrated with the flat plat solar collectors. The desired system is analyzed from the viewpoints of exergy, exergoeconomic and exergoenvironmental principles for the first time. Water/Copper oxide (CuO) nanofluid is applied as an absorbing medium inside the solar subsystem to employ solar energy effectively [36-38]. Then, the desired system is optimized by maximizing the daily exergetic efficiency and minimizing the total product cost rate as well as total product environmental impact associate with the exergy rate to find the optimum operation of desired system. Twelve parameters are selected as decision variables and NSGA-II is applied to provide the optimum solutions for four working fluids namely, R134a, R423A, R1234ze and R1234yf.

### Nomenclature

- A heat transfer area ( $\text{m}^2$ )
- b environmental impact per unit of exergy (Pts/kJ)
- $\dot{B}$  environmental impact rate associated with exergy (Pts/ h)

$Bo_{eq}$	boiling number
$c$	unit cost of exergy (\$/kJ)
$\dot{C}$	cost rate (\$/year)
$C_p$	specific heat (kJ/kg.K)
CRF	capital recovery factor
$D_h$	hydraulic diameter (m)
$\dot{E}_x$	exergy rate (kW)
$f_b$	exergoenvironmental factor
$f_c$	exergoeconomic factor
$F_R$	heat removal factor
$G_t$	total radiation rate falling on the titled collector ( $W/m^2$ )
$h$	specific enthalpy (kJ/kg)
$i$	interest rate (%)
$\dot{m}$	mass flow rate (kg/s)
$N_e$	Number
$N$	system life
$Nu$	Nusselt number

$Pr$	Prandtl number
$\dot{Q}$	heat transfer rate (kW)
$r_b$	relative environmental impacts difference
$r_c$	relative cost difference
$Re$	Reynolds number
$s$	specific entropy (kJ/kg.K)
$SH$	shape factor
$T$	temperature (K)
$U$	heat transfer coefficient (W/K.m <sup>2</sup> )
$v$	speed (m/s)
$V$	volume (m <sup>3</sup> )
$\dot{W}$	power (kW)
$X$	vapor quality
$\dot{Y}$	component-related environmental impact (Pts/h)
$Z$	capital investment and operating and maintenance cost(\$)
$\dot{Z}$	capital investment and operating and maintenance cost rate(\$/year)

## Greek letters

$\tau\alpha$  transmissivity-absorptivity product falling

$\beta$  chevron angle

$\delta$  thickness (m)

$\varepsilon$  emissivity

$\eta$  efficiency (%)

$\lambda$  thermal conductivity (W/K.m)

$\mu$  entrainment ratio

$\sigma$  Stefan-Boltzmann constant

$\rho$  density ( $\text{kg/m}^3$ )

$\phi$  maintenance factor

$\varphi$  Particles volume fraction

$\theta$  tilt angle ( $^\circ$ )

## Subscripts

0 dead state

a ambient

abs absorber

av	average
bf	base fluid
c	cold side
Col	collector
Con	condenser
d	diffuser
D	destruction
DSH	de-super heater
Eva	evaporator
ex	exergetic
F	fuel
g	glass
Gen	vapor generator
H	hot side
HE	heat exchanger
P	product
p	Pump

l	liquid phase
L	loss
LMTD	log mean temperature difference
load	load
mn	motive nozzle
ms	mixing section
net	net
nf	nanofluids
np	nanoparticles
sn	suction nozzle
sun	sun
t	top
tank	tank
Tur	turbine
u	useful
V	vaper phase
w	wind

## Superscripts

CO	construction
DI	disposal
OM	operation and maintenance
PF	environmental pollution factor

### 1. System descriptions

Fig. 1 illustrates the solar-geothermal driven CCHP system consisting of three subsystems, namely the solar collector, the geothermal and the CCHP subsystem. The solar collector subsystem is made up of solar collectors, thermal storage tank and auxiliary heater. The flat plate collector is selected to collect solar energy owing to its low cost and wide application. Pure water and water/CuO nanofluid are chosen as absorbing medium inside the solar collector subsystem. Moreover, a thermal storage tank is employed to correct the mismatch between the supply of the solar energy and the demand of thermal source consumed by the CCHP subsystem, thus the system could operate stably and continuously. The auxiliary heater is considered due to the possibility of failure in the facility for collectors and unpredictable nature of solar radiation. The geothermal subsystem consists of a heat exchanger, a pump and the geothermal well. The heat-transfer medium in the geothermal subsystem is brine. The CCHP subsystem, which mainly combines an ORC with an ejector refrigeration cycle, consists of a turbine, a de-super heater, a vapor generator, a condenser, an evaporator, an ejector, a pump, and a valve. R134a, R423A, R1234yf and R1234ze are selected as the working fluids. The ozone depletion potential (ODP)

of all desired working fluids are zero and their global warming potential (GWP) for 100 year are 1400, 2280, 6 and 4, respectively [39].

**Fig.1** Solar and Geothermal driven CCHP system

The high pressure liquid working fluid is vaporized in vapor generator by absorbing heat from the hot heat transfer medium, and then the high pressure vapor flows into the turbine where it expands to a low pressure to drive an electrical generator to produce electricity. The extracted steam from the turbine is divided into two streams. One stream is delivered to the de-super heater to provide heat load. The other stream as the primary vapor enters the supersonic nozzle of ejector. The very high velocity vapor at the exit of the nozzle produces a high vacuum at the inlet of the mixing chamber and entrains secondary vapor into the chamber from the evaporator. The two streams are mixed in the mixing chamber and become a transient supersonic stream. As the steam enters the constant cross-section zone, a normal shock wave occurs. After the shock, the mixed stream velocity becomes subsonic and decelerates in the diffuser. The stream from ejector and de-super heater enter the mixer and then flow into the condenser where they condense from vapor to a liquid by rejecting heat to the surroundings. One part of the working fluid leaving the condenser enters the evaporator after leaving the valve, and the other part flows into the geothermal heater after passing through ORC pump. In the evaporator, it is vaporized by absorbing heat from the cooled medium. Thus, a cooling effect is produced. Finally, the working fluid leaving the geothermal heater is delivered back to the vapor generator.

## 2. Working fluid selection

Selecting the convenient working fluid is the major issue for low temperature systems. Working fluids are selected considering thermophysical properties, availability, cost, stability

and environmental impact standards and so on. In this research, R134a, R423A, R1234ze and R1234yf are selected as working fluids. Table 1 represents the selected working fluids information. R134a has the desirable properties of being chemically stable, has so far indicated very low acute and chronic toxicity, has zero ozone depletion potential (ODP) and a small global warming potential (GWP) [40]. R1234yf and R1234ze, have been developed by American companies to replace R134a [41], due to their low GWPs, but they are rather expensive and difficult for wide applications in developing countries [39]. As clearly observed from Table 1, R1234yf with the minimum global warming potential is the best fluid from the environmental viewpoint. Moreover, R423A as a zeotropic working fluid with zero ODP is selected as working fluid.

**Table 1.** Properties of the selected working fluids

### 3. Methodology

#### 3.1. Energy analysis

The solar radiation is absorbed by employing flat plate solar collectors. When solar radiation passes through a transparent cover and impinges on the blackened absorber surface of high absorptivity, a large portion of this energy is absorbed by plate and transferred to the absorbing medium in fluid tubes [42]. The useful heat gain rate can be expressed as [43]:

$$\dot{Q}_u = A_{Col} F_R [G_t (\tau\alpha)_{av} - U_L (T_{nf} - T_a)] \quad (1)$$

Where,  $F_R$  represents the collector heat removal factor,  $(\tau\alpha)_{av}$  and  $G_t$  the average transmissivity-absorptivity product falling on the collector and total incident radiation on the tilted collector [43].

In Eq. (1)  $U_L$  is the overall heat loss coefficient which is the sum of bottom loss coefficient,  $U_b$ , heat loss coefficient from the collector edges,  $U_e$  and the top loss coefficient,  $U_t$ , expressed as [43].

$$U_t = \frac{1}{Ne_g} + \frac{\sigma(T_{abs}^2 + T_a^2)(T_{abs} + T_a)}{\frac{1}{\epsilon_{abs} + 0.05Ne_g(1 - \epsilon_{abs})} + \frac{2Ne_g + f - 1}{\epsilon_g} - Ne_g} \quad (2)$$

$$\frac{C}{T_{abs}} \left[ \frac{T_{abs} - T_a}{N_g + f} \right]^2 + \frac{1}{h_w}$$

where  $C$  and  $f$  are defined as follows:

$$C = 365.9(1 - 0.00883\theta + 0.000129\theta^2) \quad (3)$$

$$f = (1 - 0.04h_w + 0.0005h_w^2)(1 + 0.091Ne_g) \quad (4)$$

Here,  $\theta$  is tilt angle and  $h_w$  refers to the wind heat transfer coefficient. The insulated thermal storage tank is employed to operate as a buffer between the solar collectors and the CCHP subsystem. The absorbing medium inside the tank is assumed to be well mixed so that its temperature  $T_{nf}$  varies only with time. The Eq. (5) indicates the energy balance in the tank [23]:

$$\left[ (\rho VCp)_{nf} + (\rho VCp)_{tank} \right] \frac{dT_{nf}}{dt} = Q_u - Q_{load} - Q_L \quad (5)$$

In Eq. (5)  $Q_{load}$  and  $Q_L$  represent the energy discharged to CCHP subsystem and heat loss from tank, respectively, and can be calculated as [43], [23]:

$$Q_{load} = \dot{m}_{nf} Cp(T_{nf} - T_{nf,i}) \quad (6)$$

$$Q_L = (UA)_{tank} (T_{nf} - T_a) \quad (7)$$

water/CuO nanofluid with 0% to 3.2% particle volume concentration [37] is selected as absorbing medium inside the collector subsystem. The major reason for selecting CuO as nanoparticles is its excellent thermophysical properties at an affordable cost [44]. The nanoparticle thermophysical properties, such as density, thermal conductivity and specific heat, have also been calculated by applying Eqs. (8) to (10) [44], [38].

$$\rho_{nf} = (1 - \phi)\rho_{bf} + \phi\rho_{np} \quad (8)$$

Here,  $\phi$  is the particles volume fraction,  $\rho_{np}$  is the density of nanoparticle given to be 6000 kg/m<sup>3</sup> [37] and  $\rho_{bf}$  is the density of base fluid.

$$\frac{\lambda_{nf}}{\lambda_{bf}} = \frac{\lambda_{np} + (SH - 1)\lambda_{bf} - (SH - 1)\phi(\lambda_{bf} - \lambda_{np})}{\lambda_{np} + (SH - 1)\lambda_{bf} - \phi(\lambda_{bf} - \lambda_{np})}$$

(9)

In Eq. (9), SH is the shape factor, which is given to be 3 for the spherical shape of nanoparticle,  $\lambda_{np}$  is the thermal conductivity of nanoparticle set to be 33 W/m.K [44] and  $\lambda_{bf}$  is the thermal conductivity of base fluid.

$$Cp_{nf} = \frac{(1 - \phi)(\rho Cp)_{bf} + \phi(\rho Cp)_{np}}{\rho_{nf}} \quad (10)$$

where,  $\lambda_{bf}$  is the base fluids' specific heat and  $Cp_{np}$  indicates the nanoparticles' specific heat given to be 0.551 kJ/kg.K [37].

The CCHP subsystem is made up an organic Rankine cycle and an ejector refrigeration cycle, providing heat, power and cooling. To simplify the modelling of the CCHP subsystem, several assumptions are considered [45]:

- (1) The pressure drop in pipes or other components are neglected.
- (2) The heat loss from the heat exchangers to the environment is neglected.
- (3) The working fluid at the condenser outlet is assumed saturated liquid.
- (4) The flow through the throttle valve is isenthalpic.

The steady state energy balanced and the mass balanced are applied for each component in the CCHP subsystem by considering the above assumptions. The ejector performance simulation is carried out based on the one-dimensional constant pressure flow model. The detailed description of the ejector model is given in Ref. [45].

All the heat exchangers in this system are assumed the plate heat exchanger type for its high efficiency and compact structure [45]. In the studied heat exchanger, the working fluid works in various thermodynamic states, i.e. superheated state, two-phase state and subcooled state. In geothermal heat exchanger, the working fluid is heated undergoing the single-phase subcooled region. In the vapor generator, the working fluid respectively works in subcooled region, two-phase region and superheated region. In the condenser, the working fluid is liquefied from saturated vapor state to saturated liquid state undergoing the two-phase region. In the evaporator, however, the working fluid is vaporized only in two-phase region from saturated liquid to saturated vapor.

In the heat exchangers, the heat transfer rate in any region can be expressed as [46]:

$$Q = UA\Delta T_{LMTD} \quad (11)$$

where  $U$  is the overall heat transfer coefficient,  $A$  is heat transfer surface area,  $T_{LMTD}$  is the log mean temperature difference (LMTD) between hot side and cold side [46].

The overall heat transfer coefficient can be calculated by:

$$\frac{1}{U} = \frac{1}{h_H} + \frac{\delta_{plate}}{\lambda_{plate}} + \frac{1}{h_c} \quad (12)$$

In Eq. (12),  $h_H$  and  $h_c$  are the convection heat transfer coefficients for the hot and cold sides, respectively.  $\delta_{plate}$  and  $\lambda_{plate}$  are respectively the thickness and thermal conductivity of plate.

In Eq. (12), the heat exchanger acts under steady-state conditions. It is assumed that the heat losses and fouling effects are negligible and the flow in channels is fully developed.

$$h = \frac{\lambda Nu}{D_h} \quad (13)$$

Here,  $D_h$  refers to the hydraulic diameter of flow channel, being expressed by Ref.[46].

For the single phase region, the Nusselt number can be calculated by applying the Chisholm and Wanniarachchi correlation as follows [46]:

$$Nu = 0.724 \left( \frac{6\beta}{\pi} \right)^{0.646} Re^{0.583} Pr^{1/3} \quad (14)$$

Here,  $Re$  is Reynolds number,  $Pr$  is Prandtl number and  $\beta$  indicates the chevron angle of the plates, being expressed by Ref.[46].

For the two-phase region, the heat transfer process can be divided into small sections in which the properties can be assumed to be constant with slight property variations. The Nusselt numbers are different when the working fluid is vaporized or condensed [46].

The condensation heat transfer coefficient on the hot side for each section,  $m$ , in condenser is expressed as [46]:

$$\text{Nu}_{m,H} = \frac{h_{f,m} D_h}{\lambda_i} = 4.118 \text{Re}_{\text{eq},m}^{0.4} \text{Pr}_i^{1/3} \quad (15)$$

The evaporation heat transfer coefficient on the cold side for each section is expressed as [46]:

$$\text{Nu}_{m,c} = 1.926 \text{Pr}_i^{1/3} \text{Bo}_{\text{eq},m}^{0.3} \text{Re}^{0.5} \left[ 1 - X_m + X_m \left( \frac{\rho_l}{\rho_v} \right)^{0.5} \right] \quad (16)$$

Where  $\text{Pr}$  is the Prandtl number and  $\text{Bo}_{\text{eq}}$  stands for boiling number, being expressed by Ref. [46].

### 3.2. Ejector modeling

In this research, constant-pressure ejector is considered for proposed system owing to its better performance relative to the constant-area ejector [47] and the ejector performance simulation is performed based on the one-dimensional constant pressure flow model. For this case, by considering  $P_{10} = P_{13} = P_9 = P_{13} - \Delta P$  ( $14 \text{ kPa} \leq \Delta P \leq 50 \text{ kPa}$ ) and assuming an initial value for entrainment ratio ( $\mu$ , ejector suction mass flow rate to motive mass flow). Figure 2 illustrate the schematic of ejector.

**Fig.2** Schematic of constant-area ejector flow model

The energy equations for each section can be expressed as follows:

### 3.2.1. At the motive nozzle outlet

$$h_{9',s} = h(P_{9'}, s_{9'}) \quad (17)$$

$$h_{9'} = h_9 - \eta_{mn} (h_9 - h_{9',s}) \quad (18)$$

In Eqs. (17) and (18),  $h$  is enthalpy.  $P$  and  $s$  refer to pressure and entropy, respectively and  $\eta_{mn}$  indicates the efficiency of motive nozzle set to be 0.85.

$$v_{9'} = \sqrt{2(h_9 - h_{9'})} \quad (19)$$

$$A_{9'} = \frac{1}{(1+\mu)\rho_{9'}v_{9'}} \quad (20)$$

### 3.2.2. At the suction nozzle outlet

$$h_{13',s} = h(P_{13'}, s_{13'}) \quad (21)$$

$$h_{13'} = h_{13} - \eta_{sn} (h_{13} - h_{13',s}) \quad (22)$$

Here,  $\eta_{sn}$  is the efficiency of suction nozzle given to be 0.8.

$$A_{13'} = \frac{1}{(1+\mu)\rho_{13'}v_{13'}} \quad (23)$$

In Eq. (23),  $A$  refers to the area section.

### 3.2.3. In the mixing section

$$v_{10'} = \sqrt{\eta_{ms} \left( \frac{1}{1+\mu} v_{9'} + \frac{\mu}{1+\mu} v_{13'} \right)} \quad (24)$$

Here,  $\eta_{ms}$  refers to the efficiency of mixing section set to be 0.75.

$$h_{10'} = \frac{1}{1+\mu} \left( h_{9'} + \frac{v_{9'}^2}{2} \right) + \frac{\mu}{1+\mu} \left( h_{13'} + \frac{v_{13'}^2}{2} \right) - \frac{v_{10'}^2}{2} \quad (25)$$

$$s_{10'} = s(P_{10'}, h_{10'}) \quad (26)$$

### 3.2.4. At the diffuser outlet

$$h_{10} = h_{10'} + \frac{v_{10'}^2}{2} \quad (27)$$

$$h_{10,s} = h_{10'} - \eta_d (h_{10} - h_{10'}) \quad (28)$$

In Eq. (28),  $\eta_d$  is the efficiency of the diffuser section with value of 0.85.

$$P_{10} = P(h_{10,s}, s_{10'}) \quad (29)$$

According to the known values of  $P_9$ ,  $P_{13}$ ,  $\Delta p$ ,  $\eta_{mn}$ ,  $\eta_{sn}$ ,  $\eta_{ms}$  and  $\eta_d$ , the value of  $\mu$  can be calculated by iteration until Eq. (30) is true.

$$x_{10} = \frac{1}{1 + \mu} \quad (30)$$

In Eq. (30),  $x$  is vapor quality.

### 3.3. Exergy analysis

In the exergy analysis, the exergy balance is applied for each component of system at steady state conditions. By definition of exergy of product,  $\dot{E}x_{p,k}$ , and fuel,  $\dot{E}x_{F,k}$  for the  $k$ -th component:

$$\dot{E}x_{F,k} = \dot{E}x_{p,k} + \dot{E}x_{D,k} + \dot{E}x_{L,k} \quad (31)$$

If the system boundaries are assumed at the temperature  $T_0$  of the reference environment, the exergy losses due to heat transfer to the environment for each component are negligible,  $\dot{E}x_{L,k} = 0$  [48]. Therefore, the exergy destruction rate for each component is calculated as the difference between the fuel and the product for the component.

### 3.4. Exergoeconomic analysis

Thermoeconomics is the branch of engineering that combines exergy analysis and economic principles to provide the system designer or operator with information not available through conventional energy analysis and economic evaluations but crucial to the design and operation of a cost-effective system [49]. Thermoeconomic balance for each component is carried out based on exergy and cost balances. In a conventional economic analysis, a cost balance within the  $k$ th component is usually formulated for the overall system operating at steady state as follows [49]:

$$\sum_{\text{out}} \dot{C}_k = \sum_{\text{in}} \dot{C}_k + \dot{Z}_k \quad (32)$$

$$\dot{C} = c \cdot \dot{E}_x \quad (33)$$

In Eq. (32),  $\dot{Z}$  denotes capital investment and operating and maintenance cost rate. The cost rate of each component is calculated as [50]:

$$\dot{Z} = \frac{Z \times \phi \times \text{CRF}}{N} \quad (34)$$

where,  $Z_k$  denotes the purchase cost of the  $k$ th component listed in Table 2,  $\phi$  is the maintenance factor, CRF indicates capital recovery factor determined as [50]:

$$\text{CRF} = \frac{i(1+i)^N}{(1+i)^N - 1} \quad (35)$$

In Eq. (35)  $i$  is the interest rate and  $N$  is the system life. The values of cost parameters are listed in Table 3.

**Table 2.** Component costs [50] [51] [52] [53]

**Table 3.** cost parameters [49]

In addition, to assess the economic performance of the  $k$ th component, the exergoeconomic parameters are defined as follows [54]:

$$\dot{C}_D = c_F \dot{E}x_D \quad (36)$$

Here,  $\dot{C}_D$  and  $c_F$  refer to exergy destruction cost rate and unit cost of fuel exergy within each component of system, respectively.

$$r_c = \frac{(c_P - c_F)}{c_F} \quad (37)$$

In Eq. (37),  $r_c$  represents the relative cost difference for each component.

$$f_c = \frac{\dot{Z}}{\dot{Z} + \dot{C}_D} \quad (38)$$

where  $f_c$  is the exergoeconomic factor that indicates the ratio of the investment cost rate to the total costs rate.

### 3.5. Exergoenvironmental analysis

The exergoenvironmental analysis is considered as one of the most promising tools to assess energy-conversion processes from an environmental point of view [24]. It is an appropriate combination of the exergy analysis and the life cycle assessment (LCA) providing information about the effect of thermodynamic inefficiency on the environmental impacts.

Exergy analysis is a powerful tool for evaluating the quality of a resource as well as the location, magnitude and causes of thermodynamic inefficiencies. LCA is a technique for assessing the environmental impact associated with a product over its life cycle and it can be assessed using Eco-indicator 99. The standard Eco-indicator 99 supplies data for the production and processing

of a large number of materials, for transport processes, for disposal scenarios, etc. In addition, LCA provides the environmental impacts of a component or an overall system during its life.

For the LCA of the system being analyzed, we assumed, in analogy with the economic analysis, a life time of 15 years and 7446 working hours per year at full capacity.

The exergoenvironmental analysis for a system consists of environmental impact balances written for the  $k$ th component and auxiliary equations based on the P and F rules [24]. The environmental impact balances can be written as [55]:

$$\dot{B}_{P,k} = \dot{B}_{F,k} + (\dot{Y}_k + \dot{B}_k^{PF}) \quad (39)$$

In Eq. (39),  $\dot{Y}_k$  indicates the component-related environmental impact of component  $k$ , obtained by considering the entire life cycle of the component, i.e. (a) construction,  $\dot{Y}_k^{CO}$ , (including manufacturing, transport and installation), (b) operation and maintenance,  $\dot{Y}_k^{OM}$  and (c) the disposal,  $\dot{Y}_k^{DI}$ , of component  $k$  [55]:

$$\dot{Y}_k = \dot{Y}_k^{CO} + \dot{Y}_k^{OM} + \dot{Y}_k^{DI} \quad (40)$$

In Eq. (40),  $\dot{B}_k^{PF}$  is the environmental impact of pollutant formation within the component defined only when a chemical reaction takes place; in any other case, it is zero [55].

Exergoenvironmental balance and auxiliary equations for the system components in the current study are given in Table 4. The solution of this equation system allows us to find all the values of the environmental impact rate.

**Table 4** Exergoenvironmental balances and auxiliary equations for the system components.

Additionally, to evaluate the environmental impact performance within each component, environmental variables are defined as follows [55, 56]:

$$\dot{B}_D = b_F \dot{E}x_D \quad (41)$$

Here,  $\dot{B}_D$  is the environmental impact of exergy destruction rate and  $b_F$  refers to the environmental impact per unit of the exergy of the fuel within each component.

$$f_b = \frac{\dot{Y}}{\dot{Y} + \dot{B}_D} \quad (42)$$

In Eq. (42),  $f_b$  is the exergoenvironmental factor for each component of system.

$$r_b = \frac{b_F - b_P}{b_F} \quad (43)$$

where  $r_b$  indicates the relative environmental impact difference within each component.

#### 4. Performance criteria

Three performance parameters namely daily exergetic efficiencies, total product cost rate and total product environmental impact rate are defined in order to assess the overall system.

##### 4.1. Daily exergy efficiency

The daily exergy efficiency of the overall system for the whole day can be expressed as [57]:

$$\eta_{ex} = \frac{\int (\dot{W}_{net} + \dot{E}x_{P,Eva} + \dot{E}x_{P,DSH} + \dot{E}x_{P,Con}) d\tau}{\int (\dot{E}x_{18} + \dot{E}x_{Ph,sun}) d\tau} \quad (44)$$

where  $\dot{E}x_{18}$  is the geothermal input exergy which can be given as [57]:

$$\dot{E}x_{18} = \dot{m}_{18} [(h_{18} - h_0) - T_0 (s_{18} - s_0)] \quad (45)$$

In Eq. (45)  $\dot{E}x_{ph,sun}$  is the solar input exergy to the system which can be expressed as [58]:

$$\dot{E}x_{ph,sun} = G_t A_{Col} \left[ 1 + \frac{1}{3} \left( \frac{T_0}{T_{sun}} \right)^4 - \frac{4}{3} \left( \frac{T_0}{T_{sun}} \right) \right] \quad (46)$$

In Eq.(46)  $T_{sun}$  is the temperature of the sun, which is given to be 6000 K [58].

#### 4.2. Total product cost rate

The total product cost rate of overall system,  $\dot{C}_{P,tot}$ , is defined as sum of the product cost rates of turbine, evaporator, de-superheater and condenser:

$$\dot{C}_{P,tot} = \dot{C}_{P,Eva} + \dot{C}_{P,DSH} + \dot{C}_{P,Con} \quad (47)$$

#### 4.3. Total product environmental impact rate

The total net output related environmental impact rate for the overall system is defined as follows:

$$\dot{B}_{P,tot} = \dot{B}_{P,Eva} + \dot{B}_{P,DSH} + \dot{B}_{P,Con} \quad (48)$$

### 5. Modeling validation

In order to evaluate the accuracy of the modeling proposed in this work, the desired system was modeled in cogeneration mode, i.e. the ejector refrigeration cycle was removed, when R134a is applied as working fluid. Considering the input data listed in Table 5 [59], the results of present work can be compared with those of [59] in Table 6. According to Table 6, comparison between modeling results and those of [59] shows a good agreement.

**Table 5** Input parameters [59].

**Table 6** Results.

In order to demonstrate the superiority of the proposed CCHP system, its energetic and exergetic performance are compared with those proposed in literature. Regardless of systems configuration, when the inlet energy and exergy values are kept equal with those in Ref. [8], the thermal and exergy efficiencies for the desired system are obtained 28.7% and 42.12% which indicate respectively 83.62% and 5.88% improvements relative to the cycle proposed in Ref. [8] when R123 is selected as the working fluid. Moreover, for the same inlet energy and exergy with those considered in Ref. [9], regardless of the systems configuration, the energy and exergy efficiencies of the proposed CCHP system are calculated 38.4% and 10.29%, respectively for the R423A ( the worst working fluid from the energy and exergy viewpoints) while the thermal and exergy efficiencies obtained for proposed system in Ref. [9] are calculated 27.3% and 9.9%, respectively, i.e. 40.66% and 3.94% improvements in the daily thermal and exergy efficiencies, respectively are obtained for our proposed system. Finally, for the same input parameters with those in Ref. [14], the thermal and exergy efficiencies of the desired system are obtained 68.05% and 35.59% for the R423A which indicate 28.40% and 23.57% improvements in the cycle proposed in Ref. [14].

**6. Results and discussions**

exergy, exergoeconomic and exergoenvironmental modeling of the system have been conducted based on simulation code in Engineering Equation Solver (EES) [60]. The main thermodynamic parameters for the simulation of the desired CCHP system are listed in Table 7 and Table 8 indicates the results of the desired CCHP system simulation for all working fluids.

**Table 7** Simulation conditions for the CCHP system.

As shown in Table 8, the total input exergy is almost the same for all working fluids. The maximum daily exergy efficiency is obtained 3.000 % for R134a because of the total product exergy calculated (12.050 kW) relative to other studied fluids.

The minimum total product cost rate is obtained for R1234ze with the value of 5878 \$/year because of low product cost rate of de-superheater by the value of 774.14 \$/year relative to other studied working fluids. In addition, the working fluids R1234yf, R423A and R134a are in next ranking, respectively with the values of 5956, 6711 and 20276 \$/year, respectively.

The minimum total product environmental impact rate associated with exergy is obtained for R1234ze with the value of 44.56 Pts/h owing to the low value of product environmental impact in de-superheater (8.468 Pts/h). Moreover, the working fluids R1234yf, R423A and R134a are in next ranking, respectively with the values of 44.90, 50.74 and 126.70 Pts/h, respectively.

The small difference between the values of product environmental impact rate for R1234ze and R1234yf is owing to the portion of product environmental impact rate of de-superheater and net output power, i.e. the value of product environmental impact rate of de-superheater is 9.348 Pts/h for R1234yf while it is 8.302 Pts/h when R1234ze is used as working fluid. In addition, the portion of environmental impact of turbine net output for R1234yf is 14.62 Pts/h while it is 13.88 Pts/h for R1234ze.

**Table 8** The thermodynamic performance simulation for the CCHP system

The results of exergy, exergoeconomic and environmental analyses for each component of system are listed in Tables 9-12 for all working fluids. It is observed that the exergy destruction rate of the collector with value of 364.9 kW is dominant among all components which is due to the high temperature heat between sun and the fluid inside the collector pipes. According to Table 9, the ejector with the exergy destruction rate of 13.25 kW for R134a is in the next ranking. Moreover, for all working fluids pump2 has the highest exergy efficiency (about 94.87%). From the exergoeconomic viewpoint, the components with high value of the total costs rate, i.e.  $\dot{Z} + \dot{C}_D$ , are important. According to Table 9, the maximum value of  $\dot{Z} + \dot{C}_D$  belongs to the ejector (10255.82 \$/year) followed by the turbine and condenser with values of 5070.547\$/year and 4370.412\$/year, respectively. As observed from Table 10, the thermal storage tank with value of 2220.147\$/year has the maximum  $\dot{Z} + \dot{C}_D$  followed by the turbine and condenser, respectively. According to Tables 11 and 12, turbine with values of 2070.197\$/year and 1846.102/year, respectively are dominant. It is concluded that turbine and condenser are considerable from the exergoeconomic viewpoint for all working fluids. The infinity value of  $r_c$  for the collector is due to zero value of fuel cost. Outcomes show that evaporator has the maximum value of  $r_c$  for all working fluids which indicates the high value of product cost. It is revealed that for all working fluids, in the collector,  $f_c$  is 100% which shows that the exergy destruction cost rate within this component is zero and all costs are related to its investment and maintenance costs. Similarly, the components with high value of the total environmental impact, i.e.  $\dot{Y} + \dot{B}_D$ , are the important components from the exergoenvironmental viewpoint. As it is obvious, the ejector with value of 60.22Pts/h and thermal storage tank with value of 21.21Pts/h have the maximum environmental impact when R134a and R423A, respectively are used as working fluids. In addition, for R134ze and R1234yf, the condenser respectively with values of

14.71Pts/h and 14.101Pts/h is dominant among components. Moreover, the collector with infinity value of  $r_b$  has the maximum potential for reducing the environmental impact for all working fluids. Furthermore, for all working fluids, the maximum value of  $f_b$  is related to the collector because the environmental impact of exergy destruction rate within this component is zero and all environmental impact is due to the component-related one.

**Table 9** Results obtained from the exergy, exergoeconomic and exergoenvironmental analyses for R134a

**Table 10** Results obtained from the exergy, exergoeconomic and exergoenvironmental analyses for R423A

**Table 11** Results obtained from the exergy, exergoeconomic and exergoenvironmental analyses for R1234ze

**Table 12** Results obtained from the exergy, exergoeconomic and exergoenvironmental analyses for R1234yf

Further results indicate that applying nanoparticles in absorbing medium has a positive effect on the daily exergy efficiency of overall system for all studied fluids. Because applying the nanoparticles cause the decrement of the specific heat of base fluid. Therefore, the outlet temperature of heat transfer medium leaving the collector increases. The increment of nanoparticles leads to the decrement of the unit cost of electricity generated and the total product cost rate of heat exchangers leading to the decrement of the total product cost rate of the overall system. On the contrary, the total heat exchangers areas increase because of the decrement of heat transfer coefficient as nanoparticles increase.

Outcomes clarify that the increment of nanoparticles in the absorbing medium leads to the decrement of environmental impact per unit of the exergy of produced electricity and the product environmental impact rate of each heat exchanger. These decrements cause the decrement of

total product environmental impact rate of overall system. In addition, results indicate that the increment of nanoparticles in absorbing medium has a positive effect on the total environmental impact of exergy destruction. The maximum decrement is obtained when R134a is used as working fluid with values of 31.56% and R1234yf, R423A and R1234ze with values of 17.55%, 17.28% and 16.97% are in the next ranking.

### *6.1. Optimization results for all working fluids*

The NSGA-II method is employed to find the optimum performance of the desired system for all working fluids. Twelve key parameters, namely nanoparticles volume fraction, turbine inlet mass flow rate, pressure drop of ejector, area ratio of ejector, turbine inlet pressure, turbine outlet pressure, turbine extraction pressure, turbine outlet temperature, turbine extraction temperature, pinch temperature difference of geothermal heater, collectors area and collector tilt angle are chosen as the decision variables. The ranges of the decision variables in the optimization for various working fluids are listed in Table 13.

**Table 13** Data of the parameter optimization.

### *6.2. Single-objective optimization results for all working fluid*

In many cases of the energy system optimization, more than one objective function is considered. Often, the objective functions will be conflicting. The optimization in this section is performed for three various objective functions including the daily exergy efficiency, the total product cost rate and the total product environmental impact rate associated with exergy, i.e. Eqs. (44), (47) and (48).

In the desired system, four single objective optimizations are carried out for each working fluid because in single optimization only one especial objective can be optimized in which other objective functions may not achieve their optimal values. The optimum system performance and the corresponding combination of the decision variables are shown in Tables 14 and 15.

According to Tables 14 and 15, the maximum daily exergy efficiency is obtained for R134a with the value of 5.192%. It is clearly revealed that the minimum total product cost rate is calculated as 3255 \$/year for R1234ze and the minimum product environmental impact rate associated with exergy is obtained when R1234yf is used as a working fluid with values of 30.08 Pts/h.

Single objective optimizations of the cycle with R134a as working fluid show that the daily exergy efficiencies increase by about 73.07% and the total product environmental impact rate associated with exergy and total product cost rates decrease 68.75% and 77.92%, respectively in comparison with the base case. When R423A is applied as working fluid, the single objective optimizations lead to the increment of daily exergy efficiencies by about 85.44% and the decrement of total product environmental impact rate associated with exergy and the total product cost rates within 29.86% and 50.71%, respectively in comparison with the base case. When the R1234ze is used as the working fluid, the single objective optimizations cause the increment of daily exergy efficiencies within 92.21% and the decrement of total product environmental impact rate associated with exergy and the total product cost rate by about 19.34% and 44.62%, respectively in comparison with the base case. When R1234yf is applied as working fluid, the single objective optimizations show that daily exergy efficiencies increase about 86.3% and total product environmental impact rate associated with exergy and total product cost rates decrease within 33% and 42.68%, respectively relative to the base case.

**Table 14** Single-objective optimization results and corresponding decision variables for R134a and R423A

**Table 15** Single-objective optimization results and corresponding decision variables for R1234ze and R1234yf

### 6.3. Multi-objective optimization

In this study, NSGA-II is adopted to conduct the multi-objective optimization of desired system to find the optimal conditions with conflict objective functions.

Figs. 3 (a)-6 (a) indicate the three dimensional (3D) Pareto optimal frontier for various working fluids of multi-objective optimization. In addition, to illustrate the results of multi objective optimization with two objective functions, three two dimensional (2D) diagrams, i. e. Figs. 3 (b-d)-6 (b-d) in which the relation between two objectives from three objectives are clarified, are plotted.

**Fig. 3** Pareto optimal frontier for R134a (a) 3D, (b)-(d) 2D

**Fig. 4** Pareto optimal frontier for R423A (a) 3D, (b)-(d) 2D projection

**Fig. 5** Pareto optimal frontier for R1234ze (a) 3D, (b)-(d) 2D projection

**Fig. 6** Pareto optimal frontier for R1234yf (a) 3D, (b)-(d) 2D projection

Selection of a single optimum point from existing points on the Pareto frontier (Figs. 3-6) requires a process of decision-making. In fact, this process is mostly carried out based on engineering experiences and importance of each objective for decision makers [61]. The final decision-making process is usually performed with the aid of an ideal point. If three objective

functions would be optimized individually, i.e. disregarding another objective function, the composition of these values represents the ideal point or ideal objective point. Since the ideal point is not a solution located on the Pareto frontier, the closest point of Pareto frontier to the ideal point might be selected as final optimum solution. Before it, the objectives should be non-dimensionalized. In this paper, LINMAP method is applied to non-dimensionalize the objectives using the relation in Ref. [61].

The final value of optimum objective functions, the daily exergy efficiency, the total product environmental impact rate and the total product cost with corresponding design parameters using the above procedure are obtained for each working fluid and listed in Table 16. Also, these optimum points are illustrated for each working fluid in Figs. 3-6 using red markers. According to Table 16, it is clearly revealed that the best working fluid from the exergy viewpoint is R134a with the value of 4.194% followed by R1234yf, R1234ze and R423A, respectively with the values of 4.057%, 3.852% and 3.314%, respectively. In this case, the minimum nanoparticle volume fraction, area ratio of ejector, turbine extraction pressure, turbine outlet temperature and pinch temperature values of 0.02960, 3.459, 1000 kPa, 340 K and 5 K, respectively are required relative to other studied working fluids. Outcomes reveal that the best working fluid from the exergoeconomic viewpoint is R423A with total product cost rate of 4496 \$/year. It is observed that the working fluids R1234ze, R1234yf and R134a are in the next ranking, respectively with the values of 4675, 4787 and 5644 \$/year, respectively. In this case, the minimum turbine inlet mass flow rate, turbine extraction temperature and collector area with values of 1 kg/s, 310 K and 352 m<sup>2</sup>, respectively and the maximum turbine extraction pressure with value of 2026 kPa are needed in comparison with other fluids.

The working fluid R1234ze leads to the minimum total product environmental impact rate associated with exergy with the value of 36.82 Pts/h followed by R523A, R1234yf and R134a, respectively with the values of 36.90, 37.27 and 42.57 Pts/h, respectively. In this case, the maximum nanoparticle volume fraction, pressure drop of ejector, turbine extraction temperature, pinch temperature with values of 0.03200, 26.85 kPa, 316.2 kPa, 5.13 K, respectively and the minimum turbine inlet pressure, turbine outlet pressure, collector tilt angle and collector area with values of 2732 kPa, 582.7 kPa, 25° and 352 m<sup>2</sup>, respectively are required related to other studied working fluids.

**Table 16** The values of final optimum design parameters and objective functions for four working fluids.

The multi objective optimization leads to the improvement of the daily exergetic efficiency within 39.8% and the decrement of total product cost rate and the total product environmental impact rate by about 72.16% and 66.4%, respectively relative to the base point for R134a. For R423A, the daily exergetic efficiency increases 66.36% and the total product cost rate and the total product environmental impact rate decrease 33% and 27.28%, respectively in comparison with the base point. The optimum point for R1234ze indicates the increment of 59.57% in the daily exergetic efficiency and the decrement of 20.46% and 17.37% for the total product cost rate and environmental impact rate, respectively in comparison with the base point. Finally, when R1234yf is applied as working fluid, the daily exergetic efficiency improves by about 49.76% and the total product cost rate and environmental impact rate decrease within 19.62% and 16.99%, respectively relative to the base case.

## 7. Conclusion:

A solar-geothermal driven CCHP based on water/CuO nanofluid is modeled applying exergy, exergoeconomic and exergoenvironmental concepts. The daily exergy efficiency, the total product cost rate and the total product environmental impact rate are selected as three objective functions while twelve parameters namely, nanoparticles volume fraction, turbine inlet mass flow rate, area ratio of ejector, pressure drop of ejector, turbine inlet pressure, turbine outlet pressure, turbine extraction pressure, turbine outlet temperature, turbine extraction temperature, pinch temperature difference of geothermal heater, collector tilt angle and collectors area are selected as decision variables. The multi objective optimizations are carried out for four organic working fluids, i.e. R134a, R423A, R1234yf and R1234ze. The major conclusions obtaining from this work are summarized as follows:

- For all studied fluids, applying the nanoparticles in pure water has a positive effect on the daily exergy efficiency, the total product cost rate and the total product environmental impact rate.
- R134a is the best working fluid from the exergy point of view and R1234yf is the best working fluid from the exergoeconomic and exergoenvironmental points of view.
- For all studied fluids, the maximum daily exergy efficiency and minimum total product cost and environmental impact rates occur when collector tilt angle and collector area are close to their lower amounts.
- Optimization of R423A leads to the maximum daily exergetic efficiency at which the nanoparticle volume fraction is minimum.
- Optimization of R1234ze causes the minimum total product environmental impact rate at which the maximum nanoparticle volume fraction is required.

## References

1. Targoff, J., *Using Stirling engines for residential CHP*. ASHRAE Journal, 2008. **50**(11): p. 42.
2. Esen, H., M. Inalli, and M. Esen, *Technoeconomic appraisal of a ground source heat pump system for a heating season in eastern Turkey*. Energy Conversion and Management, 2006. **47**(9): p. 1281-1297.
3. Esen, H., M. Inalli, and M. Esen, *A techno-economic comparison of ground-coupled and air-coupled heat pump system for space cooling*. Building and environment, 2007. **42**(5): p. 1955-1965.
4. Esen, H., et al., *Energy and exergy analysis of a ground-coupled heat pump system with two horizontal ground heat exchangers*. Building and environment, 2007. **42**(10): p. 3606-3615.
5. Esen, M. and T. Yuksel, *Experimental evaluation of using various renewable energy sources for heating a greenhouse*. Energy and Buildings, 2013. **65**: p. 340-351.
6. Wu, D. and R. Wang, *Combined cooling, heating and power: a review*. progress in energy and combustion science, 2006. **32**(5): p. 459-495.
7. FRUNZULICĂ, R. and A. DAMIAN, *Small-scale cogeneration-a viable alternative for Romania*. 2008.
8. Wang, J., et al., *"A new combined cooling, heating and power system driven by solar energy"*. Renewable Energy, 2009. **34**(12): p. 2780-2788.
9. Zhai, H., et al., *"Energy and exergy analyses on a novel hybrid solar heating, cooling and power generation system for remote areas"*, in *Applied Energy*. 2009. p. 1395-1404.
10. Meng, X., et al., *Theoretical study of a novel solar trigeneration system based on metal hydrides*. Applied Energy, 2010. **87**(6): p. 2050-2061.
11. Balli, O., H. Aras, and A. Hepbasli, *"Thermodynamic and thermoeconomic analyses of a trigeneration (TRIGEN) system with a gas-diesel engine: Part I-Methodology"*. energy conversion and management, 2010. **51**(11): p. 2252-2259.
12. Balli, O., H. Aras, and A. Hepbasli, *"Thermodynamic and thermoeconomic analyses of a trigeneration (TRIGEN) system with a gas-diesel engine: Part II-An application"*. Energy Conversion and Management, 2010. **51**(11): p. 2260-2271.
13. Fang, F., et al., *Complementary configuration and operation of a CCHP-ORC system*. Energy, 2012. **46**(1): p. 211-220.
14. Wang, J., et al., *Parametric analysis of a new combined cooling, heating and power system with transcritical CO<sub>2</sub> driven by solar energy*. Applied Energy, 2012. **94**: p. 58-64.

15. Mago, P.J. and R. Luck, *Evaluation of the potential use of a combined micro-turbine organic Rankine cycle for different geographic locations*. Applied energy, 2013. **102**: p. 1324-1333.
16. Ghaebi, H., M. Saidi, and P. Ahmadi, "*Exergoeconomic optimization of a trigeneration system for heating, cooling and power production purpose based on TRR method and using evolutionary algorithm*". Applied Thermal Engineering, 2012. **36**: p. 113-125.
17. Al-Sulaiman, F.A., I. Dincer, and F. Hamdullahpur, "*Thermoeconomic optimization of three trigeneration systems using organic Rankine cycles: Part I–Formulations*". Energy Conversion and Management, 2013. **69**: p. 199-208.
18. Al-Sulaiman, F.A., I. Dincer, and F. Hamdullahpur, "*Thermoeconomic optimization of three trigeneration systems using organic Rankine cycles: Part II–Applications*". Energy Conversion and Management, 2013. **69**: p. 209-216.
19. Guo, L., et al., *A two-stage optimal planning and design method for combined cooling, heat and power microgrid system*. Energy Conversion and Management, 2013. **74**: p. 433-445.
20. Sanaye, S. and H. Hajabdollahi, *Thermo-Economic Optimization of Solar CCHP Using Both Genetic and Particle Swarm Algorithms*. Journal of Solar Energy Engineering, 2015. **137**(1): p. 011001.
21. Boyaghchi, F.A. and P. Heidarnejad, *Thermodynamic analysis and optimisation of a solar combined cooling, heating and power system for a domestic application*. International Journal of Exergy, 2015. **16**(2): p. 139-168.
22. Boyaghchi, F.A. and P. Heidarnejad, *Thermoeconomic assessment and multi objective optimization of a solar micro CCHP based on Organic Rankine Cycle for domestic application*. Energy Conversion and Management, 2015. **97**: p. 224-234.
23. Wang, M., et al., *Multi-objective optimization of a combined cooling, heating and power system driven by solar energy*. Energy Conversion and Management, 2015. **89**: p. 289-297.
24. Meyer, L., et al., *Exergoenvironmental analysis for evaluation of the environmental impact of energy conversion systems*. Energy, 2009. **34**(1): p. 75-89.
25. Boyano, A., et al., *Exergoenvironmental analysis of a steam methane reforming process for hydrogen production*. Energy, 2011. **36**(4): p. 2202-2214.
26. Petrakopoulou, F., et al., *Exergoeconomic and exergoenvironmental analyses of a combined cycle power plant with chemical looping technology*. International Journal of Greenhouse Gas Control, 2011. **5**(3): p. 475-482.
27. Petrakopoulou, F., et al., *Exergoeconomic and exergoenvironmental evaluation of power plants including CO<sub>2</sub> capture*. Chemical Engineering Research and Design, 2011. **89**(9): p. 1461-1469.
28. Atilgan, R., et al., *Environmental impact assessment of a turboprop engine with the aid of exergy*. Energy, 2013. **58**: p. 664-671.
29. Abusoglu, A. and M.S. Sedeeq, *Comparative exergoenvironmental analysis and assessment of various residential heating systems*. Energy and Buildings, 2013. **62**: p. 268-277.
30. Blanco-Marigorta, A.M., M. Masi, and G. Manfrida, *Exergo-environmental analysis of a reverse osmosis desalination plant in Gran Canaria*. Energy, 2014. **76**: p. 223-232.

31. Hamut, H., I. Dincer, and G. Naterer, *Exergoenvironmental analysis of hybrid electric vehicle thermal management systems*. Journal of Cleaner Production, 2014. **67**: p. 187-196.
32. Khoshgoftar Manesh, M., et al., *Exergoeconomic and exergoenvironmental evaluation of the coupling of a gas fired steam power plant with a total site utility system*. Energy conversion and management, 2014. **77**: p. 469-483.
33. Keçebaş, A., *Exergoenvironmental analysis for a geothermal district heating system: An application*. Energy, 2016. **94**: p. 391-400.
34. Fergani, Z., D. Touil, and T. Morosuk, *Multi-criteria exergy based optimization of an Organic Rankine Cycle for waste heat recovery in the cement industry*. Energy Conversion and Management, 2016. **112**: p. 81-90.
35. Mosaffa, A. and L.G. Farshi, *Exergoeconomic and environmental analyses of an air conditioning system using thermal energy storage*. Applied Energy, 2016. **162**: p. 515-526.
36. Yousefi, T., et al., *An experimental investigation on the effect of Al<sub>2</sub>O<sub>3</sub>-H<sub>2</sub>O nanofluid on the efficiency of flat-plate solar collectors*. Renewable Energy, 2012. **39**(1): p. 293-298.
37. Faizal, M., et al., *Energy, economic and environmental analysis of metal oxides nanofluid for flat-plate solar collector*. Energy Conversion and Management, 2013. **76**: p. 162-168.
38. Alim, M., et al., *Analyses of entropy generation and pressure drop for a conventional flat plate solar collector using different types of metal oxide nanofluids*. Energy and Buildings, 2013. **66**: p. 289-296.
39. Zhang, T. and S. Mohamed, *Conceptual Design and Analysis of Hydrocarbon-Based Solar Thermal Power and Ejector Cooling Systems in Hot Climates*. Journal of Solar Energy Engineering, 2015. **137**(2): p. 021001.
40. Huber, M.L. and M.O. McLinden, *Thermodynamic Properties of R134a (1, 1, 1, 2-tetrafluoroethane)*. 1992.
41. Ayub, Z., *Status of enhanced heat transfer in systems with natural refrigerants*. Journal of Thermal Science and Engineering Applications, 2010. **2**(4): p. 044001.
42. Wang, M., et al., *Thermodynamic analysis and optimization of a solar-driven regenerative organic Rankine cycle (ORC) based on flat-plate solar collectors*. Applied Thermal Engineering, 2013. **50**(1): p. 816-825.
43. Kalogirou, S.A., *Solar energy engineering: processes and systems*. 2013: Academic Press.
44. Khairul, M., et al., *Heat transfer performance and exergy analyses of a corrugated plate heat exchanger using metal oxide nanofluids*. International Communications in Heat and Mass Transfer, 2014. **50**: p. 8-14.
45. Wang, J., et al., *Parametric analysis and optimization of a building cooling heating power system driven by solar energy based on organic working fluid*. International Journal of Energy Research, 2013. **37**(12): p. 1465-1474.
46. Wang, J., et al., *Multi-objective optimization of an organic Rankine cycle (ORC) for low grade waste heat recovery using evolutionary algorithm*. Energy Conversion and Management, 2013. **71**: p. 146-158.
47. Li, H., et al., *Performance characteristics of R1234yf ejector-expansion refrigeration cycle*. Applied Energy, 2014. **121**: p. 96-103.

48. Lazzaretto, A. and G. Tsatsaronis, *SPECO: a systematic and general methodology for calculating efficiencies and costs in thermal systems*. Energy, 2006. **31**(8): p. 1257-1289.
49. Bejan, A. and M.J. Moran, *Thermal design and optimization*. 1996: John Wiley & Sons.
50. Ahmadi, P., I. Dincer, and M.A. Rosen, *Multi-objective optimization of a novel solar-based multigeneration energy system*. Solar Energy, 2014. **108**: p. 576-591.
51. Mohammadkhani, F., et al., *Exergoeconomic assessment and parametric study of a Gas Turbine-Modular Helium Reactor combined with two Organic Rankine Cycles*. Energy, 2014. **65**: p. 533-543.
52. Boyaghchi, F.A., M. Chavoshi, and V. Sabeti, *Optimization of a novel combined cooling, heating and power cycle driven by geothermal and solar energies using the water/CuO (copper oxide) nanofluid*. Energy, 2015. **91**: p. 685-699.
53. Purevsuren, D., *Thermoeconomic analysis of a new geothermal utilization CHP plant in Tsetserleg, Mongolia*. 2005: United Nations University.
54. Bejan, A. and G. Tsatsaronis, *Thermal design and optimization*. 1996: John Wiley & Sons.
55. Petrakopoulou, F., et al., *Environmental evaluation of a power plant using conventional and advanced exergy-based methods*. Energy, 2012. **45**(1): p. 23-30.
56. Meyer, L., et al., *Application of exergoeconomic and exergoenvironmental analysis to an SOFC system with an allothermal biomass gasifier*. International Journal of Thermodynamics, 2009. **12**(4): p. 177-186.
57. Kanoglu, M. and A. Bolatturk, *Performance and parametric investigation of a binary geothermal power plant by exergy*. Renewable Energy, 2008. **33**(11): p. 2366-2374.
58. Van Gool, W., *Energy policy: fairy tales and factualities*, in *Innovation and technology—strategies and policies*. 1997, Springer. p. 93-105.
59. Tempesti, D. and D. Fiaschi, *Thermo-economic assessment of a micro CHP system fuelled by geothermal and solar energy*. Energy, 2013. **58**: p. 45-51.
60. Solver., E.E.E., Available at: <http://www.fchart.com/>.
61. Khorasaninejad, E. and H. Hajabdollahi, *Thermo-economic and environmental optimization of solar assisted heat pump by using multi-objective particle swarm algorithm*. Energy, 2014. **72**: p. 680-690.

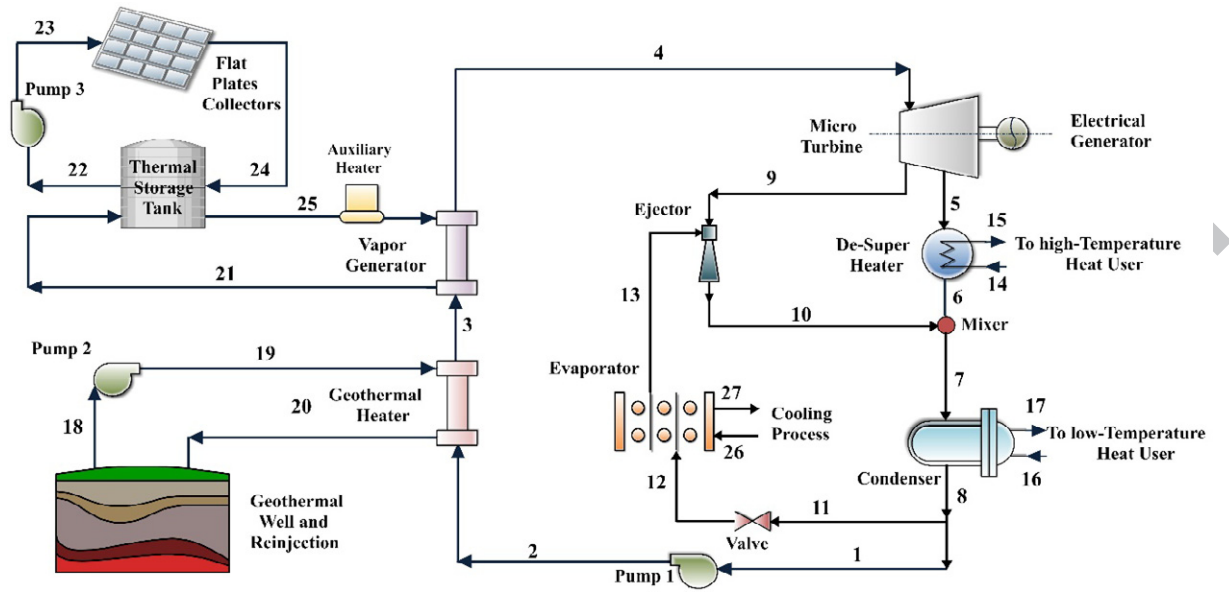


Fig.1 Solar and Geothermal driven CCHP system

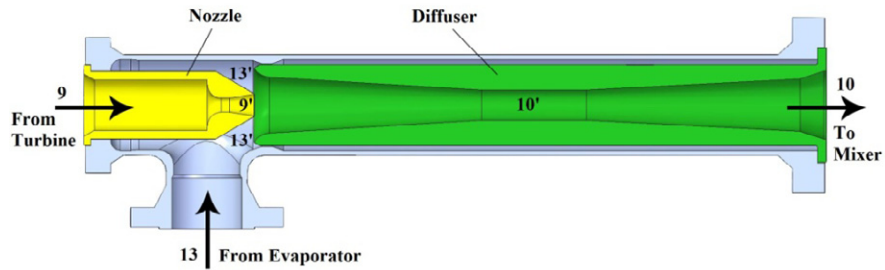
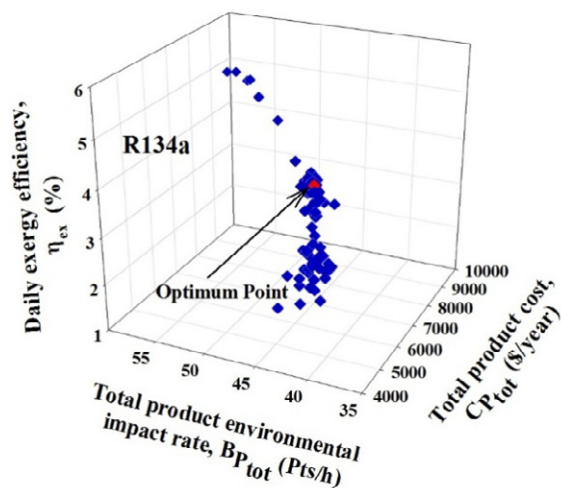
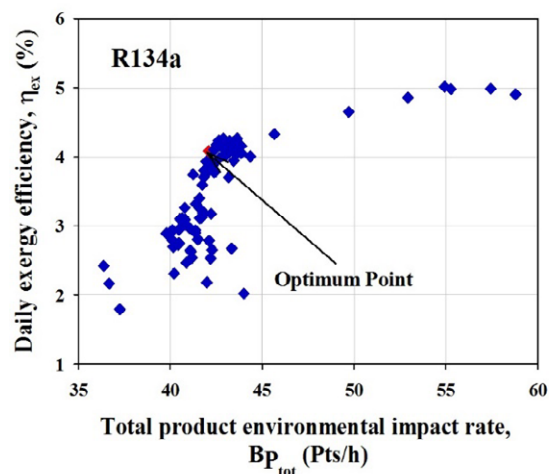


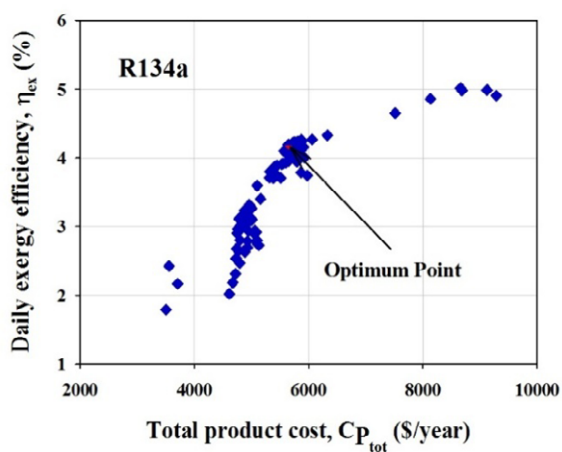
Fig.2 Schematic of constant-area ejector flow model



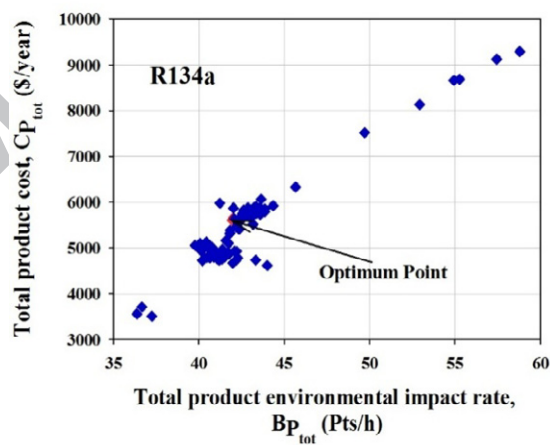
(a)



(b)



(c)



(d)

**Fig. 3** Pareto optimal frontier for R134a (a) 3D, (b)-(d) 2D

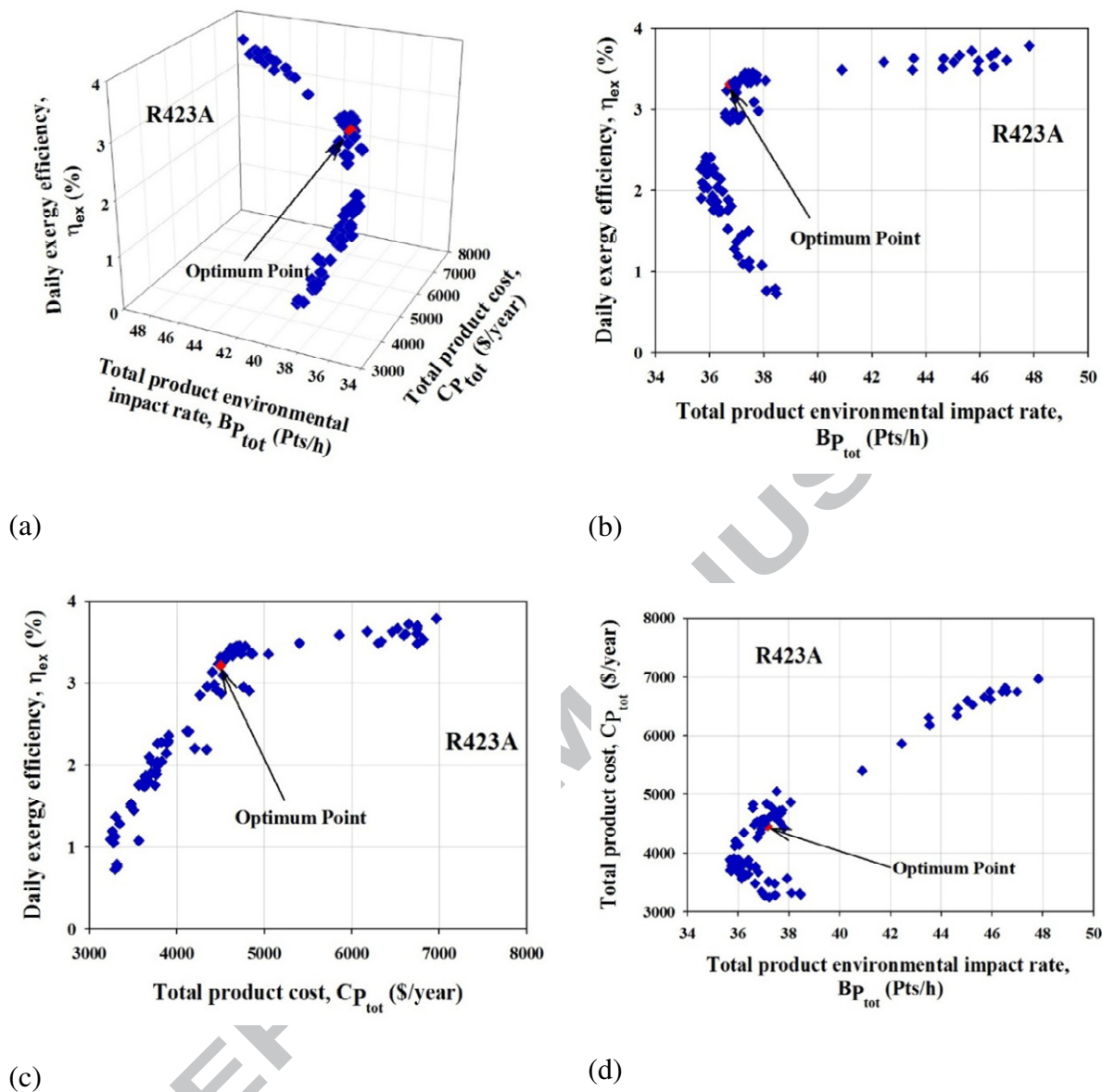
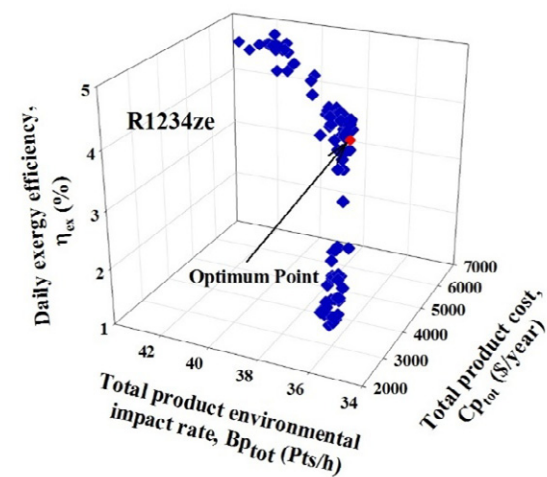
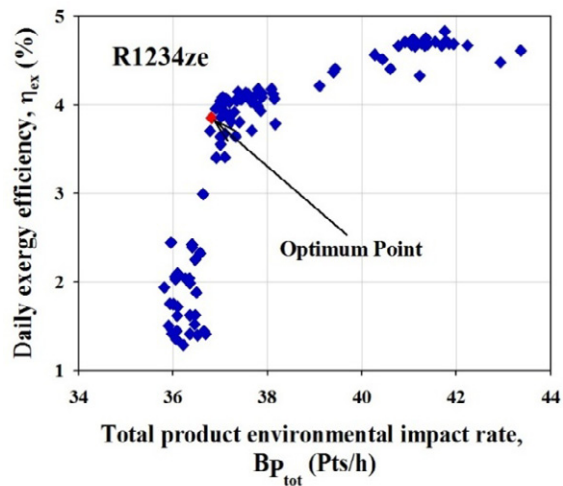


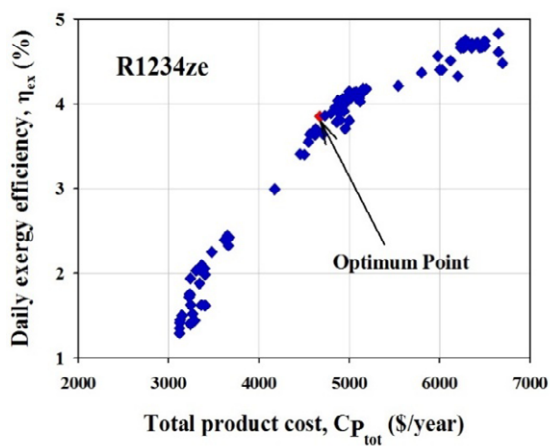
Fig. 4 Pareto optimal frontier for R423A (a) 3D, (b)-(d) 2D projection



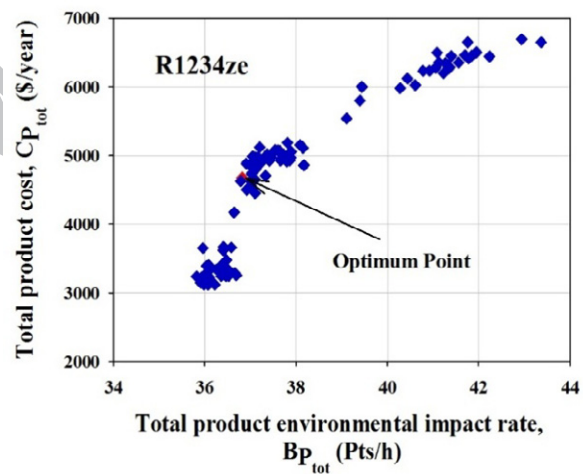
(a)



(b)

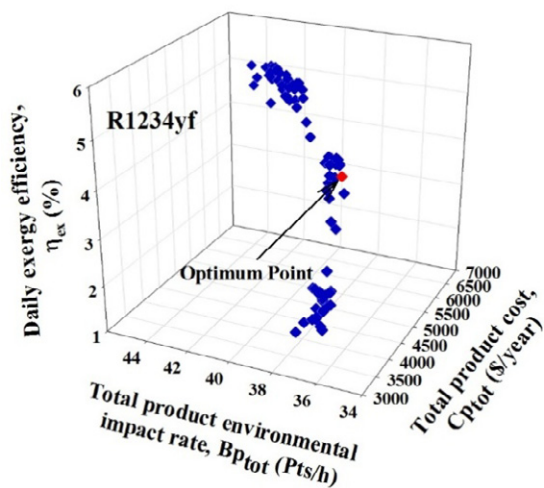


(c)

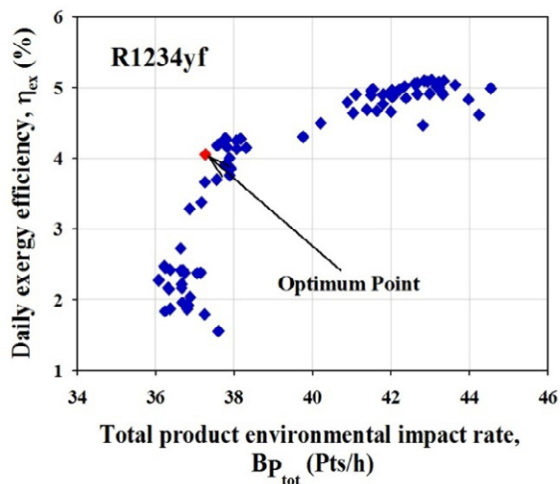


(d)

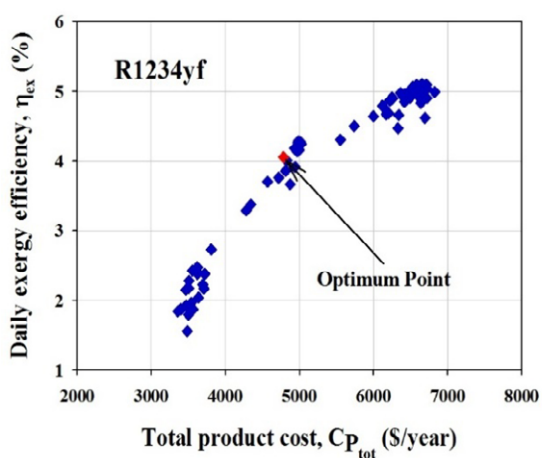
**Fig. 5** Pareto optimal frontier for R1234ze (a) 3D, (b)-(d) 2D projection



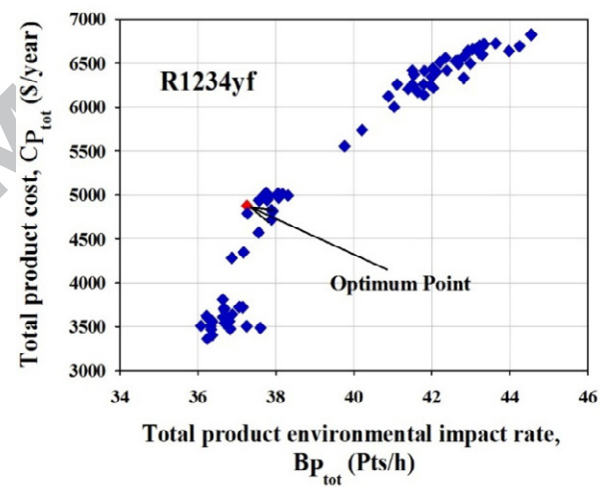
(a)



(b)



(c)



(d)

**Fig. 6** Pareto optimal frontier for R1234yf (a) 3D, (b)-(d) 2D projection

**Table 1.** Properties of the selected working fluids

Parameters	Values			
	R134a	R423A	R1234ze	R1234yf
Working fluids	R134a	R423A	R1234ze	R1234yf
Molar mass (kg/kmol)	102.03	125.96	114.04	114.04
Critical temperature (°C)	101.06	99.10	109.35	94.70
Critical pressure (kPa)	4059.30	3563	3636.30	3383.20
Normal boiling point (NBP) (°C)	-26.07	-24.14	-18.96	-29.49
ozone depletion potential (ODP)	0	0	0	0
Global warming potential (GWP) (100year)	1400	2280	6	4

**Table 2.** Component costs [50] [51] [52] [53]

Component cost	Dependent variable	Cost (\$)
Turbine	Turbine power, (kW)	$Z_{Tur} = 4750(\dot{W}_{Tur})^{0.75} + 60(\dot{W}_{Tur})^{0.95}$
Pump	Pump power, (kW)	$Z_p = 3500(\dot{W}_p)^{0.41}$
Evaporator	Heat transfer area, (m <sup>2</sup> )	$Z_{Eva} = 276 \times (A_{Eva})^{0.88}$
de-super heater, vapor generator and geothermal heater	Heat transfer area, (m <sup>2</sup> )	$Z_{HE} = 130 \left( \frac{A_{HE}}{0.093} \right)^{0.78}$
Condenser	Heat transfer area, (m <sup>2</sup> )	$Z_{Con} = 150(A_{Con})^{0.8}$
Storage tank	Heat transfer volume, (m <sup>3</sup> )	$Z_{tan k} = (1380 \times V_{tan k}) \times 0.4$
Costs of geothermal wells drilled	-	208594

**Table 3.** cost parameters [49]

Parameters	Value
Maintenance factor, $\phi$	1.06
Interest rate, $i$	15%
System life, $N$	15 year

**Table 4** Exergoenvironmental balances and auxiliary equations for the system components.

Components	Exergoenvironmental balance equations	Auxiliary equations
<b>The CCHP subsystem</b>		
<b>Turbine</b>	$b_{Tur} \dot{W}_{Tur} + b_5 \dot{E}x_5 + b_9 \dot{E}x_9 = b_4 \dot{E}x_4 + \dot{Y}_{Tur}$	$b_4 = b_5 = b_9$
<b>De-Super Heater</b>	$b_{15} \dot{E}x_{15} + b_6 \dot{E}x_6 = b_5 \dot{E}x_5 + b_{14} \dot{E}x_{14} + \dot{Y}_{DSH}$	$b_5 = b_6$
<b>Vapor Evaporator</b>	$b_{13} \dot{E}x_{13} + b_{27} \dot{E}x_{27} = b_{26} \dot{E}x_{26} + b_{12} \dot{E}x_{12} + \dot{Y}_{Eva}$	$b_{12} = b_{13}$
<b>Ejector</b>	$b_{10} \dot{E}x_{10} = b_{13} \dot{E}x_{13} + b_9 \dot{E}x_9 + \dot{Y}_{Eje}$	-
<b>Mixer</b>	$b_7 \dot{E}x_7 = b_6 \dot{E}x_6 + b_{10} \dot{E}x_{10} + \dot{Y}_{Mix}$	-
<b>Condenser</b>	$b_{17} \dot{E}x_{17} + b_8 \dot{E}x_8 = b_{16} \dot{E}x_{16} + b_7 \dot{E}x_7 + \dot{Y}_{Con}$	$b_7 = b_8$
<b>Pump1</b>	$b_2 \dot{E}x_2 = b_1 \dot{E}x_1 + b_{p1} \dot{W}_{p1} + \dot{Y}_{p1}$	-
<b>Generator</b>	$b_4 \dot{E}x_4 + b_{21} \dot{E}x_{21} = b_{25} \dot{E}x_{25} + b_3 \dot{E}x_3 + \dot{Y}_{Gen}$	$b_{21} = b_{25}$
<b>The geothermal subsystem</b>		
<b>Pump2 and Well</b>	$b_{19} \dot{E}x_{19} = b_{p2} \dot{W}_{p2} + \dot{Y}_{p2} + \dot{Y}_{Well}$	-
<b>Geothermal Heater</b>	$b_3 \dot{E}x_3 + b_{20} \dot{E}x_{20} = b_{19} \dot{E}x_{19} + b_2 \dot{E}x_2 + \dot{Y}_{GH}$	$b_{19} = b_{20}$
<b>The solar collection subsystem</b>		
<b>Storage Tank</b>	$b_{22} \dot{E}x_{22} + b_{25} \dot{E}x_{25} + b_{F,tank} \dot{E}x_L = b_{21} \dot{E}x_{21} + b_{24} \dot{E}x_{24} + \dot{Y}_{Tank}$	$b_{22} = b_{25}$
<b>Pump3</b>	$b_{23} \dot{E}x_{23} = b_{22} \dot{E}x_{22} + b_{p3} \dot{W}_{p3} + \dot{Y}_{p3}$	-
<b>Flat Plate Collector</b>	$b_{24} \dot{E}x_{24} = b_{23} \dot{E}x_{23} + b_{sun} \dot{E}x_{sun} + \dot{Y}_{sun}$	-

**Table 5** Input parameters [59].

Input parameters	Values
Turbine power output $W_{\text{Tur}}$ (kW)	50
Condenser temperature $T_1$ (K)	318
Maximum cycle temperature $T_4$ (K)	420
Geothermal temperature $T_{21}$ (K)	363
Pinch point temperature difference PP (K)	5
Ambient temperature $T_0$ (K)	284

**Table 6** Results.

Performance parameters	Ref. [59]	This study	Difference (%)
Daily thermal efficiency, $\eta_{\text{th}}$ (%)	2.946	3.071	4.24
Daily exergy efficiency, $\eta_{\text{ex}}$ (%)	39.35	39.62	0.68
Net output power, $\dot{W}_{\text{net}}$ (kW)	11.4	11.29	0.96
Total heat load $\dot{Q}_{\text{Con}} + \dot{Q}_{\text{DSH}}$ (kW)	217.35	219.03	0.77

**Table 7** Simulation conditions for the CCHP system.

<b>CCHP system</b>	<b>Fluids</b>	<b>Value</b>
Turbine inlet mass flow rate, $\dot{m}_4$ (kg/s)	All fluids	1.4
Pressure drop of ejector, $\Delta p$ (kPa)	All fluids	18
Area ratio of ejector, AR	All fluids	2
Turbine inlet pressure, $P_4$ (kPa)	R134a	3800
	R423A	3300
	R1234ze	2900
	R134yf	3000
Turbine extraction pressure, $P_9$ (kPa)	R423A	2100
	Other fluids	1300
Turbine outlet temperature, $T_5$ (K)	All fluids	350
Turbine extraction temperature, $T_9$ (K)	All fluids	305
Water flow rate at de-Super heater, $\dot{m}_{14}$ (kg/s)	All fluids	0.45
Water flow rate at condenser, $\dot{m}_{16}$ (kg/s)	All fluids	22.3
Water flow rate at evaporator, $\dot{m}_{26}$ (kg/s)	All fluids	5
<b>Collector subsystem</b>		
Nanoparticles volume fraction, $\phi$		0.00
Collector slope, $\beta$ ( $^\circ$ )		30
Collector flow rate, $\dot{m}_{23}$ (kg/s)		5.5
Storage tank number		12
Density of Steel, $\rho_{\text{Steel}}$ ( $\text{kg/m}^3$ )		8050
Conductivity of steel, $\lambda_{\text{Steel}}$ (kW/m K)		0.42
<b>Geothermal Section</b>		
Pinch temperature difference of geothermal heater, PP (K)		7
Geothermal flow rate, $\dot{m}_{18}$ (kg/s)		0.63
Water temperature outlet of geothermal well, $T_{18}$ (K)		367
<b>Environmental Condition</b>		
Simulation date		June 6
Dead state temperature, $T_0$ (K)		298
Dead state pressure, $P_0$ (kPa)		101.3
Daily total radiation on a terrestrial horizontal surface, H (kWh/m <sup>2</sup> .day)		9.29

**Table 8** The thermodynamic performance simulation for the CCHP system

Term	R134a	R423A	R1234ze	R1234yf
System inlet exergy, $\dot{E}x_{in}$ (kW)	401.60	401.30	401.10	401.10
Total product exergy, $\dot{E}x_{p,tot}$ (kW)	12.050	7.996	9.683	10.87
Daily exergy efficiency, $\eta_{ex}$ (%)	3.000	1.992	2.414	2.709
Total product cost rate, $\dot{C}_{p,tot}$ (\$/year)	20276	6711	5878	5956
Product cost rate of turbine net output, $\dot{C}_{p,T}$ (\$/year)	11185.97	3015.63	2921.81	3098.73
Product cost rate of de-superheater, $\dot{C}_{p,DSH}$ (\$/year)	2510.88	995.02	774.15	915.95
Product cost rate of condenser, $\dot{C}_{p,Con}$ (\$/year)	4929.55	2346.03	1820.37	1691.43
Product cost rate of evaporator, $\dot{C}_{p,Eva}$ (\$/year)	1647.47	352.76	361.07	249.83
Total product environmental impact rate, $\dot{B}_{p,tot}$ (Pts/h)	126.70	50.74	44.56	44.90
Product environmental impact rate of turbine net output, $\dot{B}_{p,T}$ (Pts/h)	60.78	15.24	13.79	14.62
Product environmental impact rate of de-superheater, $\dot{B}_{p,DSH}$ (Pts/h)	18.48	10.11	8.47	9.35
Product environmental impact rate of condenser, $\dot{B}_{p,Con}$ (Pts/h)	33.15	19.04	15.51	14.80
Product environmental impact rate of evaporator, $\dot{B}_{p,Eva}$ (Pts/h)	14.25	6.37	6.80	6.14

**Table 9** Results obtained from the exergy, exergoeconomic and exergoenvironmental analyses for R134a

Components	Exergetic analysis		Exergoeconomic analyses			Exergoenvironmental analysis		
	$\dot{E}_{x_D}$ (kW)	$\eta_{ex}$ (%)	$\dot{Z} + \dot{C}_D$ (\$/year)	$r_c$ (%)	$f_c$ (%)	$\dot{Y} + \dot{B}_D$ (Pts/h)	$r_b$ (%)	$f_b$ (%)
Turbine	4.874	76.4	5070.547	42.72	27.68	22.350	32.07	3.669
De-Super Heater	2.102	32.84	1737.565	224.7	8.98	6.935	306.90	33.370
Condenser	4.506	11.54	4370.412	780.1	1.742	29.860	907.9	15.570
Evaporator	1.522	0.98	1630.458	10110	0.777	14.155	1002	32.850
Pump1	0.868	80.26	1055.605	39.1	11.71	5.424	30.43	6.637
Pump2	0.014	94.87	53.600	96.93	72.82	0.439	96.67	81.970
Pump3	0.554	20.24	652.797	432.6	8.88	4.592	438.10	10.020
Ejector	13.250	54.55	10255.820	83.32	0	60.220	83.32	0
Vapor Generator	1.183	92.38	314.269	22.45	63.24	5.423	57.86	85.740
Geothermal Heater	4.259	69.7	831.215	61.63	29.47	6.424	157.40	72.380
Flat Plate Collector	364.900	4.28	1249.677	$\infty$	100	4.650	$\infty$	100
Thermal Storage Tank	0.689	94.37	1580.782	4.456	0.243	15.000	6.44	25.040

**Table 10** Results obtained from the exergy, exergoeconomic and exergoenvironmental analyses for R423A

Components	Exergetic analysis		Exergoeconomic analyses			Exergoenvironmental analysis		
	$\dot{E}_{x_D}$ (kW)	$\eta_{ex}$ (%)	$\dot{Z} + \dot{C}_D$ (\$/year)	$r_c$ (%)	$f_c$ (%)	$\dot{Y} + \dot{B}_D$ (Pts/h)	$r_b$ (%)	$f_b$ (%)
Turbine	4.867	72.14	2453.249	74.70	48.31	8.664	42.65	9.464
De-Super Heater	2.447	27.73	750.396	306.70	15.05	8.593	567.80	27.730
Condenser	7.403	5.44	2220.147	1763	1.44	18.250	2331	25.480
Evaporator	0.759	0.48	351.269	21050	1.94	6.440	76800	73.120
Pump1	0.661	80.55	411.922	68.13	26.99	1.879	49.94	19.160
Pump2	0.014	94.87	41.557	91.47	93.92	0.391	95.81	92.020
Pump3	1.847	20.24	935.623	438.50	10.15	4.606	427.40	7.816
Ejector	6.416	60.85	1686.072	64.33	0	10.600	64.33	0
Vapor Generator	0.891	94.25	266.072	15.88	61.58	5.290	50.42	87.900
Geothermal Heater	2.660	79.07	545.655	41.23	35.79	5.653	149.20	82.260
Flat Plate Collector	364.900	4.27	1249.677	$\infty$	100	4.650	$\infty$	100
Thermal Storage Tank	1.021	92.49	2696.431	6.598	0.15	21.210	8.43	18.560

**Table 11** Results obtained from the exergy, exergoeconomic and exergoenvironmental analyses for R1234ze

Components	Exergetic analysis		Exergoeconomic analyses			Exergoenvironmental analysis		
	$\dot{E}_{x_D}$ (kW)	$\eta_{ex}$ (%)	$\dot{Z} + \dot{C}_D$ (\$/year)	$r_c$ (%)	$f_c$ (%)	$\dot{Y} + \dot{B}_D$ (Pts/h)	$r_b$ (%)	$f_b$ (%)
Turbine	4.623	72.93	2070.197	85.78	56.74	6.324	42.64	12.97
De-Super Heater	2.291	28.54	596.799	336.60	25.62	7.378	677.20	63.02
Condenser	8.016	7.35	1690.549	1302	3.15	14.71	1844	31.61
Evaporator	1.408	0.93	357.927	11030	3.32	6.776	34000	68.62
Pump1	0.653	80.68	345.792	78.49	32.07	1.468	57.80	24.52
Pump2	0.014	94.87	41.943	92.94	93.11	0.383	92.94	93.97
Pump3	0.554	20.24	257.441	508.80	22.52	1.301	544.90	27.67
Ejector	2.411	88.39	475.263	13.13	0	2.922	69.34	0
Vapor Generator	1.049	93.24	278.296	25.94	32.45	5.193	179.90	77.19
Geothermal Heater	3.675	70.91	718.712	60.73	32.45	6.024	179.90	77.19
Flat Plate Collector	364.900	4.28	1249.677	$\infty$	100	4.650	$\infty$	100
Thermal Storage Tank	0.688	94.37	1199.607	4.45	0.32	12.790	6.96	29.81

**Table 12** Results obtained from the exergy, exergoeconomic and exergoenvironmental analyses for R1234yf

Components	Exergetic analysis		Exergoeconomic analyses			Exergoenvironmental analysis		
	$\dot{E}_{x_D}$ (kW)	$\eta_{ex}$ (%)	$\dot{Z} + \dot{C}_D$ (\$/year)	$r_c$ (%)	$f_c$ (%)	$\dot{Y} + \dot{B}_D$ (pts/h)	$r_b$ (%)	$f_b$ (%)
Turbine	2.939	82.10	1846.102	67.12	67.52	4.556	26.59	18
De-Super Heater	2.434	34.11	658.859	256.20	24.61	7.744	483.40	60.05
Condenser	6.966	6.89	1579.413	1407	3.94	14.101	2016	32.98
Evaporator	0.949	0.65	248.292	16050	4.48	6.127	63600	75.89
Pump1	0.664	80.66	338.072	71.93	33.02	1.428	47.73	25.20
Pump2	0.014	94.87	43.690	95.82	89.39	0.382	94.61	94.27
Pump3	0.554	20.24	246.960	515.10	23.48	1.252	553.30	28.76
Ejector	3.496	88.95	725.896	19.13	0	4.522	19.13	0
Vapor Generator	1.715	69.94	247.844	63.36	32.17	5.532	181	84.10
Geothermal Heater	3.896	69.94	755.194	63.36	32.17	6.098	181	76.26
Flat Plate Collector	364.900	4.28	1249.677	$\infty$	100	4.650	$\infty$	100
Thermal Storage Tank	0.688	94.37	1189.689	4.45	0.32	12.744	6.98	29.93

**Table 13** Data of the parameter optimization.

Term	Type of fluids	Value
Nanoparticles volume fraction, $\phi$	All fluids	0-0.032
Turbine inlet mass flow rate, $\dot{m}_4$ (kg/s)	All fluids	1-1.5
Pressure drop of ejector, $\Delta P$ (kPa)	All fluids	14-27
Area ratio of ejector, AR	All fluids	2-3.5
Turbine inlet pressure, $P_4$ (kPa)	R134a	3400-3900
	R423A	2900-3400
	R1234ze	2500-3000
	R134yf	2800-3300
Turbine outlet pressure, $P_5$ (kPa)	R1234ze	550-850
	Other fluids	750-1050
Turbine extraction pressure, $P_9$ (kPa)	R423A	2000-3000
	Other fluids	1000-2000
Turbine outlet temperature, $T_5$ (K)	All fluids	340-360
Turbine extraction temperature, $T_9$ (K)	All fluids	300-317
Pinch temperature difference of geothermal heater, PP (K)	All fluids	5-10
Collector tilt angle, $\theta$ ( $^\circ$ )	All fluids	25-34
Collectors area, $A_c$ ( $m^2$ )	All fluids	352-475.2

**Table 14** Single-objective optimization results and corresponding decision variables for R134a and R423A

Objective functions	R134a			R423A		
	$\eta_{ex,max}$	$\dot{C}_{P,tot,min}$	$\dot{B}_{P,tot,min}$	$\eta_{ex,max}$	$\dot{C}_{P,tot,min}$	$\dot{B}_{P,tot,min}$
Daily exergy efficiency, $\eta_{ex}$ (%)	<b>5.192</b>	2.005	2.841	3.694	0.680	2.187
Total product cost, $\dot{C}_{P,tot}$ (\$/year)	9547	4476	5165	6337	3308	4283
Total product environmental impact rate, $\dot{B}_{P,tot}$ (Pts/h)	59.45	43.55	39.59	44.15	38.56	35.59
<b>Decision variables</b>						
Nanoparticles volume fraction, $\phi$	0.03200	0.03131	0.03171	0.02733	0.00471	0.03200
Turbine inlet mass flow rate, $\dot{m}_4$ (kg/s)	1.493	1.002	1.001	1.481	1.025	1.011
Area ratio of ejector, AR	3.492	3.497	3.462	3.491	2.000	3.343
Pressure drop of ejector, $\Delta P$ (kPa)	27.00	26.45	25.65	24.50	25.64	24.10
Turbine inlet pressure, $P_4$ (kPa)	3589	3409	3833	3351	2905	3085
Turbine outlet pressure, $P_5$ (kPa)	750.0	1038.0	1045.0	750.0	1046.0	1047.0
Turbine outlet pressure, $P_9$ (kPa)	1000	1876	1321	2000	2927	2100
Turbine outlet temperature, $T_5$ (K)	357.9	340.3	340.5	340.0	359.4	340.0
Turbine extraction temperature, $T_9$ (K)	300.0	316.1	316.0	300.9	316.2	301.5
Pinch temperature difference of geothermal heater, PP (K)	5.003	9.093	5.178	5.044	9.949	5.348
Collector tilt angle, $\theta$ ( $^\circ$ )	25.01	25.05	25.51	25.11	33.69	28.20
Collectors Area, $A_C$ (m <sup>2</sup> )	352.7	360.3	475.2	353.0	352.2	475.2

**Table 15** Single-objective optimization results and corresponding decision variables for R1234ze and R1234yf

Objective functions	R1234ze			R1234yf		
	$\eta_{ex,max}$	$\dot{C}_{P,tot,min}$	$\dot{B}_{P,tot,min}$	$\eta_{ex,max}$	$\dot{C}_{P,tot,min}$	$\dot{B}_{P,tot,min}$
Daily exergy efficiency, $\eta_{ex}$ (%)	4.640	1.382	2.233	5.047	1.480	2.506
Total product cost, $\dot{C}_{P,tot}$ (\$/year)	7242	<b>3255</b>	3629	6956	3414	3557
Total product environmental impact rate, $\dot{B}_{P,tot}$ (Pts/h)	45.74	36.51	35.94	45.29	37.37	<b>30.08</b>
<b>Decision variables</b>						
Nanoparticles volume fraction, $\phi$	0.03200	0.01792	0.02838	0.03194	0.00144	0.02880
Turbine inlet mass flow rate, $\dot{m}_4$ (kg/s)	1.459	1.001	1.004	1.477	1.012	1.021
Area ratio of ejector, AR	2.479	3.262	3.486	2.900	3.166	3.450
Pressure drop of ejector, $\Delta P$ (kPa)	14.00	27.00	26.80	17.17	24.30	22.94
Turbine inlet pressure, $P_4$ (kPa)	2975	2552	2867	3072	2869	2817
Turbine outlet pressure, $P_5$ (kPa)	550.3	850.0	802.0	751.8	1045.0	765.8
Turbine outlet pressure, $P_9$ (kPa)	1001	1978	1293	1001	2000	1034
Turbine outlet temperature, $T_5$ (K)	356.1	342.9	342.9	359.4	340.2	357.3
Turbine extraction temperature, $T_9$ (K)	300.0	316.6	317.0	300.3	316.6	316.1
Pinch temperature difference of geothermal heater, PP (K)	5.185	9.762	7.670	5.061	9.616	5.853
Collector tilt angle, $\theta$ (°)	25.01	30.56	33.38	27.12	32.72	32.07
Collectors Area, $A_C$ (m <sup>2</sup> )	352.0	372.6	352.6	352.0	356.8	475.2

**Table 16** The values of final optimum design parameters and objective functions for four working fluids.

<b>Objective functions</b>	<b>R134a</b>	<b>R423A</b>	<b>R1234ze</b>	<b>R1234yf</b>
Daily exergy efficiency, $\eta_{ex}$ (%)	<b>4.194</b>	3.314	3.852	4.057
Total product cost rate, $\dot{C}_{P,tot}$ (\$/year)	5644	<b>4496</b>	4675	4787
Total product environmental impact, $\dot{B}_{P,tot}$ (Pts/h)	42.57	36.90	<b>36.82</b>	37.27
<b>Decision variables</b>				
Nanoparticles volume fraction, $\phi$	0.02960	0.03164	0.03200	0.02975
Turbine inlet mass flow rate, $\dot{m}_4$ (kg/s)	1.001	1.000	1.007	1.008
Area ratio of ejector, AR	3.459	3.500	3.470	3.500
Pressure drop of ejector, $\Delta P$ (kPa)	26.71	24.28	26.85	24.01
Turbine inlet pressure, $P_4$ (kPa)	3400	3288	2732	3131
Turbine outlet pressure, $P_5$ (kPa)	750.0	753.8	582.7	775.0
Turbine extraction pressure, $P_9$ (kPa)	1000	2026	1007	1004
Turbine outlet temperature, $T_5$ (K)	340.0	340.1	340.2	346.2
Turbine extraction temperature, $T_9$ (K)	312.0	310.7	316.2	311.5
Pinch temperature difference of geothermal heater, PP (K)	5.000	5.071	5.130	5.031
Collector tilt angle, $\theta$ (°)	25.94	25.72	25.00	27.70
Collectors Area, $A_C$ (m <sup>2</sup> )	353.6	352.0	352.0	354.6

**Highlights:**

- A solar- geothermal CCHP is modeled using exergoeconomic and exergoenvironmental concepts.
- $\eta_{ex}$ ,  $\dot{C}_{P,tot}$  and  $\dot{B}_{P,tot}$  are selected as objective functions with twelve decision variables.
- The increment of nanoparticles volume fraction has a positive effect on all objective functions.
- NSGA-II is applied individually for R134a, R423A, R1234ze and R134yf.